NASA MEMO 1-5-59E

NASA

MEMORANDUM

ESTIMATED PERFORMANCE OF RADIAL-FLOW EXIT NOZZLES FOR AIR IN CHEMICAL EQUILIBRIUM

By Gerald W. Englert and Fred D. Kochendorfer

Lewis Research Center
Cleveland, Ohio

NATIONAL AERONAUTICS AND SPACE ADMINISTRATION

WASHINGTON

February 1959

NATIONAL AERONAUTICS AND SPACE ADMINISTRATION

MEMORANDUM 1-5-59E

ESTIMATED PERFORMANCE OF RADIAL-FLOW EXIT NOZZLES FOR AIR IN CHEMICAL EQUILIBRIUM

By Gerald W. Englert and Fred D. Kochendorfer

SUMMARY

The thrust, boundary-layer, and heat-transfer characteristics were computed for nozzles having radial flow in the divergent part. The working medium was air in chemical equilibrium, and the boundary layer was assumed to be all turbulent. Stagnation pressure was varied from 1 to 32 atmospheres, stagnation temperature from 1000° to 6000° R, and wall temperature from 1000° to 3000° R. Design pressure ratio was varied from 5 to 320, and operating pressure ratio was varied from 0.25 to 8 times the design pressure ratio.

Results were generalized independent of divergence angle and were also generalized independent of stagnation pressure in the temperature range of 1000° to 3000° R. A means of determining the aerodynamically optimum wall angle is provided.

INTRODUCTION

In general, the most important characteristic of an exhaust nozzle for a propulsion device is the amount of thrust that it supplies at a given pressure ratio, stagnation temperature, and stagnation pressure. This number is usually compared with the performance of an ideal nozzle; that is, a nozzle that isentropically expands the exhaust gas to free-stream pressure and a purely axial direction at its exit station. Calculations to determine the ratio of actual to ideal thrust generally depend on pressure or temperature level of the process even if viscosity is neglected; this is due to changes in specific heat and molecular weight of the working fluid. At moderately high temperatures the amount of heat transfer becomes important for structural considerations so that the boundary layer, which in turn determines the heat-transfer coefficient, can no longer be neglected. Since nozzle exit angle and design pressure ratio (or area ratio) also must be considered, the selection of an optimum nozzle for a particular application becomes a sizeable task.

The figures of this report were prepared to reduce repetitious computation of thrust and heat-transfer characteristics of radial-flow nozzles using air as a working medium. The general trends and order of magnitude of viscous effects may aid in the selection of nozzles using fluids other than air. Boundary-layer momentum thickness and form factor are also included as a possible aid to those engaged in developing separation triggering devices. Radial-flow nozzles are defined herein as nozzles that have all the potential-flow velocity vectors of the divergent section directed radially outward as if originating from a point source located ahead of the nozzle throat. All the potential-flow properties are therefore constant on any spherical surface with center at the hypothetical point source. The bounding walls of the divergent sections are conical. The convergent sections considered are those plotted in figure 1.

All calculations are based on air at chemical equilibrium with a composition of 20.95 percent oxygen, 78.09 percent nitrogen, 0.93 percent argon, and 0.03 percent carbon dioxide at standard conditions. Calculations were made for nozzles having design pressure ratios of 5 to 320 and inlet stagnation temperatures and pressures from 1000° to 6000° R and 1 to 32 atmospheres, respectively. Although inlet stagnation temperature of 1000° R is well below that of much practical application, it is in the range of readily available laboratory air supply and therefore in the range of considerable experimentation. Comparison of the low- and high-temperature calculation may then aid in the utilization of low-temperature data to high-temperature applications. Nozzle wall temperature was held constant at 1000°, 2000°, and 3000° R. These constant wall temperatures correspond either to the case of a heavy-walled nozzle when the longitudinal transfer of heat can be very large compared with that flowing through the boundary layer or to the case of a nozzle having coolant flow distributed to hold wall temperature constant. The boundary layers calculated were assumed to be all turbulent.

SYMBOLS

A	area on a spherical surface (fig. 1)
a	speed of sound
B	coefficient in eq. (3)
F	thrust in a direction parallel to nozzle axis
g	gravitational constant
H	profile parameter, δ^*/θ

h enthalpy

L length

M Mach number

m rate of mass flow

Pr Prandtl number

p pressure

Q rate of total heat transfer

q rate of heat transfer per unit area

R radial distance from hypothetical point source in radial flow

r distance normal to nozzle axis

T temperature

U velocity

W rate of weight flow

X transformed distance along nozzle wall

x distance along nozzle wall

Y transformed distance normal to nozzle wall

y distance normal to nozzle wall

α angle between velocity vector and axis of nozzle

γ ratio of specific heats

δ boundary-layer thickness

δ^* boundary-layer thickness displacement $= \int_0^{\delta} \left(1 - \frac{\rho U}{\rho_p U_p}\right) dy$

Θ temperature parameter $= \frac{T_s - T_w}{T_t - T_w}$

θ boundary-layer momentum thickness $= \int_0^{\delta} \frac{\rho U}{\rho_p U_p}\left(1 - \frac{U}{U_p}\right) dy$

μ absolute viscosity

ν kinematic viscosity

σ gas constant

ρ mass density

Subscripts:

av average

aw adiabatic wall

b base

e inside nozzle at exit station

g expression independent of nozzle size and wall angles

I ideal

i incompressible or transformed

opt optimum

p potential stream

ref reference

s stagnation

std standard conditions (for pressure, 1 atm)

T total

t potential-stream stagnation

v viscous

w wall

∞ undisturbed free-stream conditions external of nozzle

1 1 foot

Superscript:

* refers to nozzle throat except when used with displacement thickness

ANALYSIS

The flow through the nozzles was considered in two parts: a potential flow in the major part of the nozzle, and a boundary layer in which viscosity and conductivity were considered. The charts of reference 1 were used to determine pressures, temperatures, and enthalpies of the air in the potential-flow region. The flow direction and static pressure normal to the flow direction were considered constant in the boundary layer, so that nozzle wall pressures were determined by the potential flow.

The calculations for the development of the viscous layer of air along the walls were based on air with a constant molecular weight and essentially constant specific heat but with the proper boundary conditions at the edge of the potential layer. Some inherent inaccuracy in the upper temperature levels considered therefore may be present in the heat-transfer and boundary-layer data presented.

Basic Equations

Thrust ratio and boundary layer. - Ideal thrust coefficient F_I is defined as the thrust obtained by a nozzle expanding in all-isentropic flow to ambient pressure (p_∞) with all the terminating velocity vectors in an axial direction at the nozzle exit. Also, by definition, the actual and ideal nozzles must pass the same amount of air per unit of time.

The total mass flow through the actual and/or ideal nozzle is

$$m = \int_0^{A_w} \rho_p U_p \, dA - \int_{A_w - A_\delta}^{A_w} (\rho_p U_p - \rho U) dA$$

where A is the area on a spherical surface with the center at the hypothetical point source of the radial flow and the subscript on A denotes the boundary of A.

Utilizing the definition of displacement thickness gives:

$$m = \int_0^{A_w} \rho_p U_p \, dA - 2\pi r_w \delta^* \rho_p U_p = \int_0^{A_{\delta^*}} \rho_p U_p \, dA$$

where second-order terms of the boundary-layer parameters are neglected, so that

$$r_w \delta^* \approx (r_w - \delta^*)\delta^*$$

The quantity $A_{\delta}*$ is herein the flow area of a nozzle with all-potential flow, whereas the actual nozzle radius must be increased by δ^* to keep the rate of mass flow the same in both cases.

The actual jet thrust can be written in integral form as

$$F_T = \int_0^{A_w} \rho U^2 \cos \alpha \, dA + \int_0^{A_w} (p - p_\infty)\cos \alpha \, dA$$

where all terms except p_∞ are evaluated inside the nozzles at the exit station. It is convenient to separate F_T into potential-flow and viscous-flow components as follows:

$$F_T = \int_0^{A_{\delta}*} \rho_p U_p^2 \cos \alpha \, dA + \int_{A_{\delta}*}^{A_w} \rho_p U_p^2 \cos \alpha \, dA -$$

$$\int_{A_\delta}^{A_w} (\rho_p U_p^2 - \rho U U_p + \rho U U_p - \rho U^2)\cos \alpha \, dA +$$

$$\int_0^{A_{\delta}*} (p - p_\infty)\cos \alpha \, dA + \int_{A_{\delta}*}^{A_w} (p - p_\infty)\cos \alpha \, dA$$

so that

$$\frac{F_T}{F_I} = \frac{\left[mU_p + (p - p_\infty)A_{\delta}*\right]\cos_{av}\alpha - 2\pi r_w\left[\rho_p U_p^2 \theta - (p - p_\infty)\delta^*\right]\cos \alpha_w}{mU_I}$$

$$= \frac{F_p}{F_I} - \frac{F_v}{F_I} \tag{1}$$

The potential-flow calculations were always made normal to a spherical control surface and were resolved into the axial-flow direction by multiplying by the average cosine of the angle between the flow direction and the nozzle axis. The development in appendix A shows that

$$\cos_{av}\alpha = \frac{1 + \cos \alpha_w}{2} \tag{2}$$

for a radial-flow nozzle having circular cross sections normal to the axis.

Momentum thickness was computed by combining equations (20) and (23) of reference 2 to give

$$\theta = \left(\frac{T_t}{T_p}\right)^3 \left[\frac{0.01173}{\left(\frac{a_t}{\nu_t}\right)^{0.2155} M_p^{B+0.2155} r_w^{1.2155}} \int_0^x \frac{M_p^B \left(\frac{T_p}{T_{ref}}\right)^{0.732} r_w^{1.2155}}{\left(\frac{T_t}{T_p}\right)^{3.268}} dx \right]^{0.823} \tag{3}$$

where

$$B = 4.2 + 1.563\left(\frac{h_w}{h_t} - 1\right)$$

and T_{ref} is evaluated by h_{ref} and reference 1, where

$$\frac{h_{ref}}{h_p} = \frac{1}{2}\left(\frac{h_w}{h_p} + 1\right) + 0.22\left(\frac{h_{aw}}{h_p} - 1\right)$$

and

$$\frac{h_{aw}}{h_p} = 1 + \frac{\gamma - 1}{2} M_p^2 (Pr)_{ref}^{1/3}$$

Form factor $H = \delta^*/\theta$ was estimated by the expression

$$H = \frac{h_t + 1.286h_w}{h_p} - 1 \tag{4}$$

which is developed in appendix B.

Substituting the continuity equation

$$m = \frac{\pi(r_w - \delta^*)^2 \rho_p U_p}{\cos_{av}\alpha}$$

and equation (4) in equation (1) results in

$$\frac{F_T}{F_I} = \frac{U_p + g(p - p_\infty)\frac{A_{\delta^*}}{W}}{U_I} \cos_{av}\alpha - \left[\frac{U_p - g(p - p_\infty)\frac{A_{\delta^*}}{W}\left(\frac{h_t + 1.286h_w}{h_p} - 1\right)}{U_I} \right] \frac{2\theta}{(r_w - \delta^*)} \cos_{av}\alpha \cos \alpha_w \tag{5}$$

Heat transfer. - Combining equations (27) and (28) of reference 2 results in the following expression for rate of heat transfer per unit area:

$$q = \frac{0.123e^{-2.007\left(\frac{T_p}{T_{ref}}\right)^{0.732}} (Pr)_{ref}^{-2/3} \rho_p U_p (h_{aw} - h_w)}{\left(\frac{T_t}{T_p}\right)^{0.268} \left(\frac{M_p a_t \theta}{\nu_t}\right)^{0.268}} \tag{6}$$

The total rate of heat transfer from the nozzle is

$$Q = 2\pi \int_0^x r_w q \, dx \tag{7}$$

Generalization of Results Independent of Nozzle Size and Wall Angle

Thrust and boundary layer. - The expression

$$\frac{1}{\cos_{av}\alpha} \frac{F_p}{F_I} = \frac{U_p + g(p - p_\infty)}{U_I} \frac{A_\delta^*}{W} \equiv \left(\frac{F_p}{F_I}\right)_g \tag{8}$$

is independent of nozzle size (scale) and wall angle.

It is desirable to generalize F_v/F_I also. Let L_1 and L_2 be the distances of boundary-layer travel along the convergent and divergent section, respectively, of the nozzle. Assume that the boundary layer is all turbulent and that it has zero thickness at the entrance to the convergent section. Dividing all terms in equation (3) by $L = L_1 + L_2$ results in

$$\frac{\theta}{L^{0.823}} = \left(\frac{T_t}{T_p}\right)^3 \left[\frac{0.01173}{\left(\frac{a_t}{\nu_t}\right)^{0.2155} M_p^{B+0.2155} \left(\frac{r_w}{L}\right)^{1.2155}} \int_0^{x/L} \frac{M^{1.} \left(\frac{T_p}{T_{ref}}\right)^{0.732} \left(\frac{r_w}{L}\right)^{1.2155}}{\left(\frac{T_t}{T_p}\right)^{3.268}} d\left(\frac{x}{L}\right) \right]^{0.823} \tag{9}$$

From figure 1(b),

$$L_2 = \frac{r_w - r_w^*}{\sin \alpha_w} = \frac{\left(\sqrt{\frac{A_w}{A_w^*}} - 1\right) r_w^*}{\sin \alpha_w}$$

if radial flow is assumed at the throat.

Consider the family of convergent nozzles having lengths $L_1 \propto r_w^*/\sin \alpha_w$, such as sketched in figure 1(b). The convergent section is stretched as α_w decreases, so that any increment of length ΔL before stretching results in a length $\Delta L' = (\sin \alpha/\sin \alpha')\Delta L$ after stretching. Then, for a fixed A_w/A_w^*, $L \propto \frac{r_w^*}{\sin \alpha_w}$, or arbitrarily using $\alpha_w = 15^\circ$ and $r_w^* = r_1^* \equiv$ a 1-foot nozzle throat radius as a reference point,

$$L \propto \frac{r_w^* \sin 15^\circ}{r_1^* \sin \alpha_w} \tag{10}$$

From equation (9),

$$\theta \left(\frac{r_1^* \sin \alpha_w}{r_w^* \sin 15^\circ}\right)^{0.823} \tag{11}$$

is independent of nozzle size (scale) and wall angle. Use of expression (11) in equation (5) then shows that

$$\frac{F_v}{F_I}\left(\frac{r_w^*}{r_1^*}\right)^{0.177}\left(\frac{\sin \alpha_w}{\sin 15^\circ}\right)^{0.823} \frac{1}{\cos_{av}\alpha \cos \alpha_w} \equiv \left(\frac{F_v}{F_I}\right)_g \tag{12}$$

is independent of nozzle size and wall angle for the family of nozzles of figure 1(b).

Wall angle for optimum thrust. - For radial-flow nozzles, an increase of wall angle decreases the axial components of thrust but also decreases the thrust loss due to viscosity. An optimum wall angle for maximum total thrust F_T is therefore obtainable. Combining expressions (2), (8), and (12) gives

$$\frac{F_T}{F_I} = \frac{F_p}{F_I} + \frac{F_v}{F_I}$$

$$= \left(\frac{F_p}{F_I}\right)_g \frac{1 + \cos \alpha_w}{2} - \left(\frac{F_v}{F_I}\right)_g \left(\frac{r_1^*}{r_w^*}\right)^{0.177} \left(\frac{\sin 15^\circ}{\sin \alpha_w}\right)^{0.823} \frac{(\cos \alpha_w)(1 + \cos \alpha_w)}{2}$$

Differentiating F_T/F_I with respect to α_w and setting the result equal to zero yields

$$\left(\frac{r_1^*}{r_w^*}\right)^{0.177} \frac{\left(\frac{F_v}{F_I}\right)_g}{\left(\frac{F_p}{F_I}\right)_g} = \frac{\sin^{2.823} \alpha_{w,opt}}{(\sin 15^\circ)^{0.823}\left[\left(\sin^2 \alpha_{w,opt}\right)\left(0.177 + 1.177 \cos \alpha_{w,opt}\right) + 0.823\left(1 + \cos \alpha_{w,opt}\right)\right]} \quad (13)$$

Equation (13) is plotted in figure 2 so that, if $\left(\frac{r_1^*}{r_w^*}\right)^{0.177} \frac{\left(\frac{F_v}{F_I}\right)_g}{\left(\frac{F_p}{F_I}\right)_g}$ is known, the optimum wall angle can be determined.

Heat transfer. - Use of expression (11) in (6) indicates

$$\frac{q}{\left(\frac{r_1^*}{r_w^*} \frac{\sin \alpha_w}{\sin 15^\circ}\right)^{0.221}} \quad (14)$$

is independent of nozzle size and wall angle.

Using expressions (10) and (14) in (7) gives generalized Q as

$$\frac{Q}{\left(\frac{r_w^*}{r_1^*}\right)^{1.779} \left(\frac{\sin 15^\circ}{\sin \alpha_w}\right)^{0.779}} = 2\pi \int_{\frac{x}{L}=0}^{1} r_1^* \left(\frac{r_w}{r_w^*}\right) \frac{q}{\left(\frac{r_1^*}{r_w^*} \frac{\sin \alpha_w}{\sin 15^\circ}\right)^{0.221}} d\left(\frac{x}{\frac{\sin 15^\circ}{\sin \alpha_w} \frac{r_w^*}{r_1^*}}\right)$$

(15)

Generalization of Results Independent of Stagnation Pressure

When stagnation temperature is in the range $1000^\circ \leqq T_T \leqq 3000^\circ$ R, pressure has no effect on specific heat. In this range, however, the ratio of specific heats decreases with increase of temperature because of increases in the amount of the total internal energy content of the air molecules going into vibrational energy. Molecular weight is constant throughout this range. When temperature is increased much beyond 3200° R, molecular weight and specific heat both vary with pressure as well as with temperature (ref. 1).

Thrust and boundary layer. - Potential-flow thrust ratio can be written in terms of pressure ratio and thus is independent of stagnation pressure p_t for $1000^\circ \leqq T_t \leqq 3000^\circ$ R. With equation (1),

$$\frac{F_p}{F_I} = \frac{U_p + g(p - p_\infty)\frac{A}{w}}{U_I} \cos_{av}\alpha$$

or

$$\frac{F_p}{F_I}\frac{1}{\cos_{av}\alpha} = \left(\frac{F_p}{F_I}\right)_g = \frac{\frac{\gamma_p p}{p_t} M_p^2 + \left(\frac{p}{p_t} - \frac{p_\infty}{p_t}\right)}{\frac{\gamma_p p}{p_t} M_p M_I \sqrt{\frac{\gamma_I T_I}{\gamma_p T_p}}}$$

In this lower temperature range, pressure enters into the momentum-thickness equation (eq. (3)) only through the kinematic viscosity term and can be factored out as:

$$\theta = \left(\frac{T_t}{T_p}\right)^3 \left[\frac{0.01173(\sigma T_t)^{0.2155}}{\left(\frac{a_t}{\mu_t}\right)^{0.2155}} \int_0^x \frac{M_p^B \frac{\left(\frac{T_p}{T_{ref}}\right)^{0.732}}{\left(\frac{T_t}{T_p}\right)^{3.268}} r_w^{1.2155}\, dx}{M_p^{B+0.2155} r_w^{1.2155}} \right]^{0.823} \left(\frac{1}{p_t}\right)^{0.177}$$

Therefore,

$$\theta \propto \left(\frac{1}{p_t}\right)^{0.177} \tag{16}$$

and combining with expression (11) results in

$$\theta (p_t)^{0.177} \left(\frac{r_1^* \sin \alpha_w}{r_w \sin 15^\circ}\right)^{0.823}$$

being independent of wall angle, sizes, and pressure in the lower temperature range.

Profile parameter is independent of pressure in this temperature range. Pressure enters into the viscous-thrust-loss expression, therefore, only as

$$\left(\frac{1}{p_t}\right)^{0.177}$$

since

$$\frac{F_v}{F_I} = \frac{\left[\rho_p U_p^2 - (p - p_\infty)H\right]2\theta}{(r - \delta^*)\rho_p U_p U_I} \cos_{av}\alpha \cos \alpha_w$$

$$= \frac{\left[\frac{\gamma_p p}{p_t} M_p^2 - \left(\frac{p}{p_t} - \frac{p_\infty}{p_t}\right)H\right]2\theta}{(r_w - \delta^*)\frac{\gamma_p p}{p_t} M_p M_I \sqrt{\frac{\gamma_I T_I}{\gamma_p T_p}}} \cos_{av}\alpha \cos \alpha_w$$

and

$$\frac{F_v}{F_I} \propto \left(\frac{1}{p_t}\right)^{0.177}$$

Using equation (12) results in the expression

$$\left(\frac{F_v}{F_I}\right)_g p_t^{0.177} = \frac{F_v}{F_I} \frac{(r_w^* p_t)^{0.177}}{(\sin 15^\circ)^{0.823}} \frac{\sin \alpha_w^{0.823}}{(\cos_{av}\alpha)(\cos \alpha_w)}$$

which is independent of nozzle size and wall angles as well as pressure in the lower temperature range (1000° to 3000° R).

Heat transfer. - Using expression (16) and the equation of state in equations (6) and (7) shows that

$$q \propto p_t^{0.779}$$

and

$$Q \propto p_t^{0.779}$$

in the lower temperature range.

Therefore, from expressions (14) and (15),

$$q\left(\frac{r_w^*}{\sin \alpha_w}\right)^{0.221} p_t^{-0.779}$$

and

$$Q \frac{(\sin \alpha_w)^{0.779}}{r_w^{*1.779}} p_t^{-0.779}$$

are independent of nozzle size, wall angle, and stagnation pressure in the lower temperature range. In the presentation of the lower temperature range computations, p_t is arbitrarily divided by $2p_{std}$ to make it dimensionless in these parameters.

DISCUSSION OF RESULTS

Thrust

Potential flow. - The thrust ratio obtainable from potential flow through radial-flow nozzles was computed for nozzle design pressure ratios of 5, 10, 20, 40, 80, 160, and 320. Thrust ratio is obtained from figure 3 by multiplying the ordinate by the $\cos_{av}\alpha$ of the nozzle being considered. This average cosine of the flow direction can be obtained from equation (2).

The thrust curves are characterized by their rapid drop as the operating pressure ratio is decreased below design pressure ratio,

$$\frac{\dfrac{p_t}{p_\infty}}{\left(\dfrac{p_t}{p_\infty}\right)_{design}} = \frac{\dfrac{p_t}{p_\infty}}{\dfrac{p_t}{p_e}} = \frac{p_e}{p_\infty} < 1,$$

and by their relatively constant value as p_e/p_∞ is increased above 1. The curves have this characteristic shape even when plotted on a logarithmic scale for p_e/p_∞.

In general, thrust coefficient decreased with increase of stagnation temperature T_t when the nozzles were overexpanded ($p_e/p_\infty < 1$), this effect becoming more pronounced as either design pressure ratio or exit static pressure ratio is decreased. Only negligible effects of T_t on this potential-flow thrust ratio were found for underexpanded nozzles.

Above 4000° R stagnation temperature, the potential-flow thrust curves become more sensitive to p_e/p_∞ as p_t is decreased. The most pronounced effect found is for a nozzle designed for a pressure ratio of 5 when operated at an exit static pressure ratio of 0.24 and 6000° R stagnation temperature. Thrust ratio in this extreme case is reduced almost 20 percent as the stagnation pressure is reduced from 32 to 2 atmospheres.

Viscous flow. - Curves showing the viscous-thrust-loss parameter are also presented in figure 3. The ratio F_V/F_I is obtained after selecting α_w and r_w^*. Similar to the potential-flow thrust curves, these curves also show the greatest change with the variables considered when p_e/p_∞ is less than 1. The thrust-loss parameter always increased with decrease of exit static-pressure ratio.

Optimum wall angle. - Figure 4 is presented to indicate how much thrust decreases with deviation of nozzle wall angle α from its value for maximum thrust; the carets mark the peaks of the curves. Thrust decreases more rapidly with decrease of α below an aerodynamic optimum than it does with increase of α above optimum. Only small differences in this rate of decrease with changes of stagnation pressure or temperature, wall temperature, design pressure ratio, or exit static-pressure ratio were found.

The potential-flow thrust ratio (eq. (8)) is also shown in figure 4 (dashed line) so that the amount of thrust loss due to exit flow angle and off-design expansion can be compared with that due to viscosity. At a p_e/p_∞ of 1, the two losses are the same order of magnitude. At $p_e/p_\infty \approx 0.25$ and $\alpha_w \approx 2$, both losses are large; but, at $p_e/p_\infty \approx 8$ and $\alpha_w \approx 20$, the viscous losses are much smaller than that of the potential stream.

Optimum wall angle in figure 5 is shown to decrease with increase of exit static-pressure ratio, design pressure ratio, stagnation pressure, and wall temperature and to increase with increase of stagnation temperature. Only sample plots are shown in figure 5, since optimum wall angle can be easily obtained by use of equation (13) if figure 3 is available for the desired conditions.

Boundary-Layer Characteristics

Momentum thickness. - Momentum thickness (eq. (3)) was found to increase with increase of stagnation temperature and with decrease of wall temperature in the lower temperature range of 1000° to 3000° R (fig. 6).

In the upper temperature range, momentum thickness decreased with increase of stagnation temperature, wall temperature, or stagnation pressure. Values for the convergent part of the nozzle are shown only for the lowest stagnation pressure because of their crossing over the curves of the divergent part of the nozzle.

Profile parameter. - Profile parameter (eq. (4)) is shown in figure 7. The increase of profile parameter with increasing wall temperature and decreasing stagnation temperature is obvious from equation 4. No appreciable effect of stagnation pressure was found for $1000^{\circ} \leqq T_t \leqq 4000^{\circ}$ R. This effect of pressure appeared to be random and, since the scatter was less than 4 percent, only a mean line was shown in this temperature range. At temperatures much in excess of 4000° R, the profile parameter is consistently increased with increase of stagnation pressure.

Heat Transfer

The heat-transfer rate per unit area is shown in figure 8, and the heat-transfer rate through the whole nozzle is shown in figure 9. The curves are shown for the convergent as well as the divergent part of the nozzle. The maximum heat flux is shown to be at, or slightly downstream of, the nozzle throat. Both figures show the expected increase of heat transfer to the nozzle with increasing stagnation pressure or temperature and with decreasing wall temperature. Figures 8 and 9 are both for a constant wall temperature. Figure 10 presents the adiabatic wall temperature, that is, for the case of no heat transfer in either the x or y directions. The ratio of adiabatic wall temperature to stagnation temperature is seen to decrease with increase of stagnation temperature and with increase of stagnation pressure when $T_0 \geqq 4000^{\circ}$ R.

Valid Range of Exit Static Pressure Ratio on Charts

In practically all applications of an exit nozzle, a base region due to structural considerations will exist between the external airstream and the exhaust jet from the nozzle. The pressure in this base region, p_b, is the pressure to which the nozzle exhausts and can be, therefore, of prime importance in determining the internal flow of an overexpanded nozzle. The undisturbed external pressure p_∞ enters into the thrust equation by definition of jet thrust. When the nozzle is surrounded by still air, no difference exists between p_b and p_∞. When the nozzle is surrounded by a moving external airstream, however, as in flight, the base pressure is an involved function of the geometry of the vehicle encompassing the nozzle as well as a function of the nozzle internal and external streams. This problem is discussed in reference 3.

As operating pressure ratio p_t/p_∞ is increased above the design pressure ratio ($p_e/p_\infty = 1$) by decreasing ambient pressure p_∞ and holding inlet stagnation pressure constant, the flow inside the now-underexpanded nozzle will remain the same, and no additional computational difficulties are encountered. The thrust ratio F/F_I varies, however, as the ideal thrust varies with operating pressure ratio or p_e/p_∞. Downstream of the nozzle exit, the flow will continue to expand until it reaches ambient pressure.

As the operating pressure ratio is decreased below design pressure ratio by increasing p_∞ and holding p_t constant, the flow inside the now-overexpanded nozzle will remain essentially the same as long as the shock that is then present stays at the exit station of the nozzle. Since the flow inside the nozzle then remains an accelerating flow, it tends to stabilize the boundary layer. The exit shock will not, therefore, start to move into the nozzle until the nozzle operating pressure ratio is reduced low enough so that the pressure ratio p_e/p_b across the shock is large enough to separate the boundary layer. If the nozzle pressure ratio is decreased still further, the shock will move upstream into the nozzle and drastically alter the internal flow. At this point the charts of this report are no longer valid. When the shock is still at the exit station, any disturbance of this shock on upstream conditions is considered to have a negligible effect on nozzle performances. The charts are therefore valid for

$$\frac{p_e}{p_\infty} \geq \frac{\dfrac{p_b}{p_\infty}}{\left(\dfrac{p_b}{p_e}\right)_{\text{separation}}}$$

Theoretical and experimental evidence of reference 4 indicates that the pressure ratio required to separate an adiabatic turbulent boundary layer at a moderate temperature level must be at least as strong as the static pressure that occurs across a shock at a Mach number ratio of 0.762. Reference 5 concludes that there is no effect of heat transfer on turbulent boundary-layer separation over the range of T_w/T_t from 0.75 to adiabatic. This result was obtained from schlieren photographs of the flow over a forward-facing step (collar) mounted on an axisymmetric cooled body mounted in a supersonic wind tunnel. Additional data obtained at the Lewis Research Center from photographs of flow over a step mounted on a cooled cone indicated no effect of heat transfer even at a T_w/T_t of 0.25 (fig. 11(a)). Figure 11(b) shows the corresponding separation pressure ratio for various Mach numbers ahead of the shock; this figure was computed from oblique shock charts and a constant Mach number ratio across the shocks of 0.762.

Only a value of p_b/p_∞ is then required to estimate the pressure ratio at which a nozzle will first separate, since

$$\frac{\frac{p_t}{p_\infty}}{\left(\frac{p_t}{p_\infty}\right)_{design}} = \frac{p_e}{p_\infty} = \frac{\frac{p_b}{p_\infty}}{\frac{p_b}{p_e}}$$

and

$$\left(\frac{p_e}{p_\infty}\right)_{separation} = \frac{\frac{p_b}{p_\infty}}{\left(\frac{p_b}{p_e}\right)_{separation}}$$

SUMMARY OF RESULTS

The thrust, boundary-layer, and heat-transfer characteristics of a family of radial-flow nozzles were computed. Stagnation pressure was varied from 1 to 32 atmospheres, stagnation temperature from 1000° to 6000° R, and wall temperature from 1000° to 3000° R. All calculations were made for air in chemical equilibrium. The results, where desired, were generalized independent of wall angle.

The following results were obtained:

1. There was no effect of stagnation pressure on profile parameter, adiabatic wall temperature, or potential-flow thrust ratio of the nozzles up to a stagnation temperature of 3200° R. Beyond this temperature, profile parameter decreased, adiabatic wall temperature increased, and the potential-flow thrust curves became more sensitive to off-design pressure ratios as stagnation pressure was decreased.

2. Total thrust decreased more rapidly with decrease of wall angle below the value for maximum thrust than with increase of wall angle above that for maximum thrust. Optimum wall angle decreased with increase of exit static pressure ratio, design pressure ratio, stagnation pressure, and wall temperature; and it increased with increase of stagnation temperature.

3. The maximum heat flux was near the nozzle throat. Both total heat transfer through the nozzle and heat transfer per unit area increased with increasing stagnation pressure or temperature and with decreasing wall temperature.

Lewis Research Center
National Aeronautics and Space Administration
Cleveland, Ohio, October 15, 1958

APPENDIX A

DERIVATION OF AVERAGE COSINE OF ANGLE BETWEEN POTENTIAL-FLOW VELOCITY VECTORS AND NOZZLE AXIS

In radial flow, all flow properties are a function only of R, where R is the radius vector from the hypothetical point source to any spherical surface with the point source as center (fig. 1(a)). Therefore, mass flow per unit area, as well as force per unit area, is constant at any given radius R if area is taken in one of the aforementioned spherical surfaces. Thrust in a direction parallel to the nozzle axis is

$$F = \int_0^A \rho U^2 \cos \alpha \, dA + \int_0^A (p - p_\infty) \cos \alpha \, dA$$

where the symbols without subscripts are taken at the nozzle exit station. By definition,

$$F = \left[2\pi \int_0^{r_w} \frac{\rho U^2 r}{\cos \alpha} \, dr + 2\pi \int_0^{r_w} \frac{(p - p_\infty) r}{\cos \alpha} \, dr \right] \cos_{av} \alpha$$

$$= 2\pi \int_0^{r_w} \rho U^2 r \, dr + 2\pi \int_0^{r_w} (p - p_\infty) r \, dr$$

where

$$dA = \frac{2\pi r}{\cos \alpha} \, dr$$

Solving for $\cos_{av}\alpha$ and using the relation $r = R \sin \alpha$ gives

$$\cos_{av}\alpha = \frac{\int_0^{r_w} r \, dr}{\int_0^{r_w} \frac{r \, dr}{\cos \alpha}} = \frac{\int_0^{\alpha_w} \sin \alpha \cos \alpha \, d\alpha}{\int_0^{\alpha_w} \sin \alpha \, d\alpha} = \frac{1 + \cos \alpha_w}{2} \qquad (2)$$

APPENDIX B

DETERMINATION OF PROFILE PARAMETER

The compressible, adiabatic boundary-layer equations can be reduced to the incompressible form by use of a Stewartson-type transformation (ref. 6).

$$\left.\begin{aligned} X &= \int_0^x \frac{p_p}{p_t}\frac{a_p}{a_t}\,dx \\ Y &= \frac{a_p}{a_t}\int_0^y \frac{\rho}{\rho_t}\,dy \\ U_i &= U\frac{a_t}{a_p} \end{aligned}\right\} \tag{B1}$$

Effects of compressibility can therefore be studied by use of these transformation equations (refs. 7 to 9).

Reference 9 indicated that the incompressible profile parameter H_i is constant at a flat-plate value in a nozzle with all favorable pressure gradient $\left(\frac{dp}{dx} < 0\right)$. In this reference, H_i was obtained by operating on the measured compressible profile parameter H with a Stewartson transformation. It is assumed herein that the incompressible profile parameter $H_i = \frac{\delta_i^*}{\theta_i}$ is constant at a value of 1.286, which corresponds to a 1/7-power profile, where

$$\delta_i^* = \int_0^{\delta_i}\left(1 - \frac{U_i}{U_{i,p}}\right)dY \tag{B2}$$

$$\theta_i = \int_0^{\delta_i}\frac{U_i}{U_{i,p}}\left(1 - \frac{U_i}{U_{i,p}}\right)dY \tag{B3}$$

When nonadiabatic flow such that there is heat transfer through the boundary layer is considered, an additional integral term arises in the transformation process. The purpose of this appendix is to discuss a basis for the evaluation of this term. The resulting equations for H are the same as (9) and (25) of reference 2 if H_i is held constant, but

the derivation herein for this special case does not employ as involved or empirical a procedure. It is hoped that the following will add clarity to the assumptions involved.

Displacement thickness for compressible flow is defined as

$$\delta^* = \int_0^\delta \left(1 - \frac{\rho U}{\rho_p U_p}\right) dy$$

$$= \int_0^\delta \frac{T_p}{T}\left(\frac{T}{T_p} - \frac{U}{U_p}\right) dy \tag{B4}$$

by using the equation of state and assuming molecular weight and static pressure constant with respect to distance normal to the wall. Then, if specific heat is constant,

$$\frac{T}{T_p} = \frac{T_s}{T_t}\left(1 + \frac{\gamma - 1}{2} M_p^2\right) - \frac{\gamma - 1}{2} M_p^2 \left(\frac{U}{U_p}\right)^2 \tag{B5}$$

where T_s is the stagnation temperature corresponding to the static temperature T. Substituting equation (B5) in (B4) and making use of (B1), as in reference 4,

$$\delta^* = \int_0^\delta \frac{T_p}{T}\left[\frac{T_s}{T_t} + \frac{\gamma - 1}{2} M_p^2 \frac{T_s}{T_t} - \frac{\gamma - 1}{2} M_p^2 \left(\frac{U}{U_p}\right)^2 - \frac{U}{U_p}\right] dy$$

$$= \frac{p_t}{p_p}\frac{a_p}{a_t}\left\{\int_0^{\delta_i}\left(\frac{T_s}{T_t} - 1\right) dY + \delta_i^* + \frac{\gamma - 1}{2} M_p^2 \left[\int_0^{\delta_i}\left(\frac{T_s}{T_t} - 1\right) dY + \delta_i^* + \theta_i\right]\right\}$$

and

$$\frac{\delta^*}{\theta} = H = \frac{\int_0^{\delta_i}\left(\frac{T_s}{T_t} - 1\right) dY}{\theta_i} + H_i + \frac{\gamma - 1}{2} M_p^2 \left[\frac{\int_0^{\delta_i}\left(\frac{T_s}{T_t} - 1\right) dY}{\theta_i} + H_i + 1\right] \tag{B6}$$

where momentum thickness transforms as

$$\theta = \theta_i\left(\frac{p_t}{p_p}\frac{a_p}{a_t}\right)$$

and the integral $\int_0^{\delta_i}\left(\frac{T_s}{T_t} - 1\right)dY$ remains to be evaluated.

Incompressible turbulent boundary layers have velocity profiles that can be quite closely approximated by the relation $\frac{U_i}{U_{p,i}} = \left(\frac{Y}{\delta_i}\right)^n$ (ref. 10). It can be shown (ref. 11) for a flat plate in incompressible flow (H_i = constant) that, if $\frac{U_i}{U_{p,i}} = \left(\frac{Y}{\delta_i}\right)^n$ is a solution to the boundary-layer momentum equation, then $\frac{T_s - T_w}{T_t - T_w} = \left(\frac{Y}{\delta_i}\right)^n$ is a solution of the energy equation when Prandtl number is 1. This follows from the fact that the energy equation, when written in terms of $\Theta = \frac{T_s - T_w}{T_t - T_w}$, has the same form and boundary conditions as the momentum equation. Therefore,

$$\delta_i \int_0^1 \left(\frac{T_s}{T_t} - 1\right) d\left(\frac{Y}{\delta_i}\right) = \delta_i \frac{T_w}{T_t} \int_0^1 \left[1 - \left(\frac{Y}{\delta_i}\right)^n\right] d\left(\frac{Y}{\delta_i}\right) - \delta_i \int_0^1 \left[1 - \left(\frac{Y}{\delta_i}\right)^n\right] d\left(\frac{Y}{\delta_i}\right)$$

$$= \delta_i \frac{n}{n+1}\left(\frac{T_w}{T_t} - 1\right) \tag{B7}$$

Also,

$$H_i = \frac{\frac{\delta_i^*}{\delta_i}}{\frac{\theta_i}{\delta_i}} \frac{\int_0^1 \left[1 - \left(\frac{Y}{\delta_i}\right)^n\right] d\left(\frac{Y}{\delta_i}\right)}{\int_0^1 \left(\frac{Y}{\delta_i}\right)^n \left[1 - \left(\frac{Y}{\delta_i}\right)^n\right] d\left(\frac{Y}{\delta_i}\right)} = \frac{\frac{n}{n+1}}{\frac{n}{(n+1)(2n+1)}} = 2n + 1$$

$$= 1.286 \quad \text{if} \quad n = \frac{1}{7} \tag{B8}$$

Substituting equations (B7) and (B8) into (B6) yields

$$H = \frac{\delta_i}{\delta_i^*} \frac{n}{n+1}\left(\frac{T_w}{T_t} - 1\right) H_i + H_i + \frac{\gamma - 1}{2} M_p^2 \left[\frac{\delta_i}{\delta_i^*} \frac{n}{n+1}\left(\frac{T_w}{T_t} - 1\right) H_i + H_i + 1\right]$$

$$= \frac{T_t + 1.286 T_w}{T_p} - 1 = \frac{h_t + 1.286 h_w}{h_p} - 1 \tag{4}$$

REFERENCES

1. Moeckel, W. E., and Weston, Kenneth C.: Composition and Thermodynamic Properties of Air in Chemical Equilibrium. NACA TN 4265, 1958.

2. Reshotko, Eli, and Tucker, Maurice: Approximate Calculation of the Compressible Turbulent Boundary Layer with Heat Transfer and Arbitrary Pressure Gradient. NACA TN 4154, 1957.

3. Cortright, Edgar M., Jr.: Some Aerodynamic Considerations of Nozzle-Afterbody Combinations. Aero. Eng. Rev., vol. 19, no. 9, Sept. 1956, pp. 59-65.

4. Reshotko, Eli, and Tucker, Maurice: Effect of a Discontinuity on Turbulent Boundary-Layer-Thickness Parameters with Application to Shock-Induced Separation. NACA TN 3454, 1955.

5. Czarnecki, K. R., and Sinclair, Archibald R.: A Note on the Effect of Heat Transfer on Peak Pressure Rise Associated with Separation of Turbulent Boundary Layer on a Body of Revolution (NACA RM-10) at a Mach Number of 1.61. NACA TN 3997, 1957.

6. Stewartson, K.: Correlated Incompressible and Compressible Boundary Layers. Proc. Roy. Soc. (London), ser. A, vol. 200, no. A1060, Dec. 22, 1949, pp. 84-100.

7. Cohen, Clarence B., and Reshotko, Eli: Similar Solutions for the Compressible Laminar Boundary Layer with Heat Transfer and Pressure Gradient. NACA Rep. 1293, 1956. (Supersedes NACA TN 3325.)

8. Cohen, Clarence B., and Reshotko, Eli: The Compressible Laminar Boundary Layer with Heat Transfer and Arbitrary Pressure Gradient. NACA Rep. 1294, 1956. (Supersedes NACA TN 3326.)

9. Englert, Gerald W.: Estimation of Compressible Boundary-Layer Growth over Insulated Surfaces with Pressure Gradient. NACA TN 4022, 1957.

10. Tetervin, Neal, and Lin, Chia Chiao: A General Integral Form of the Boundary-Layer Equation for Incompressible Flow with an Application to the Calculation of the Separation Point of Turbulent Boundary Layers. NACA Rep. 1046, 1951. (Supersedes NACA TN 2158.)

11. Reynolds, W. C., Kays, W. M., and Kline, S. J.: Heat Transfer in the Turbulent Incompressible Boundary Layer. I - Constant Wall Temperature. NASA MEMO 12-1-58W, 1958.

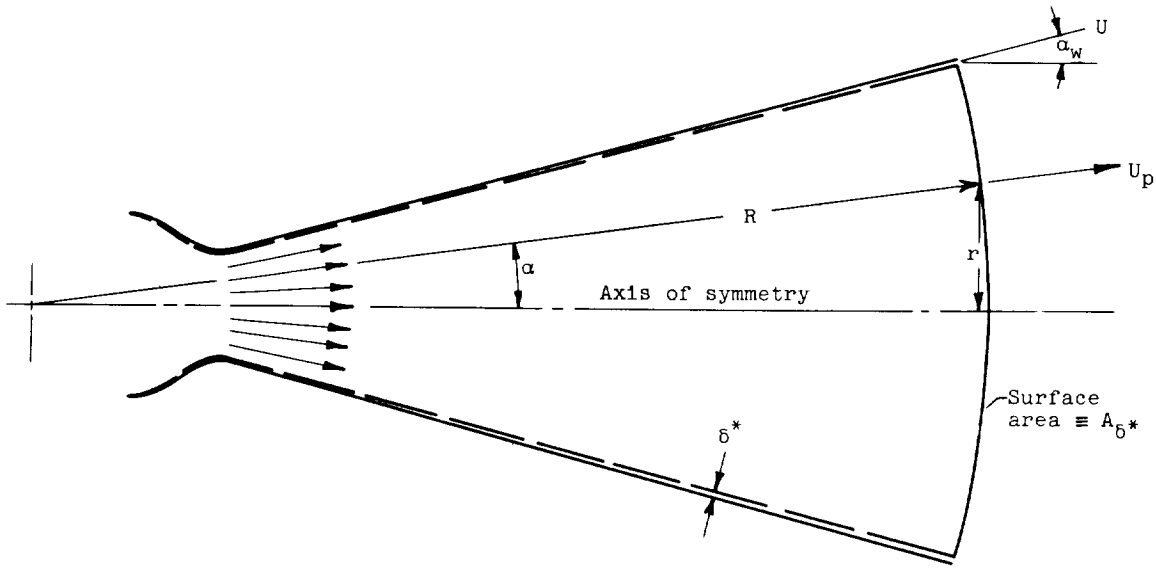

(a) Flow model.

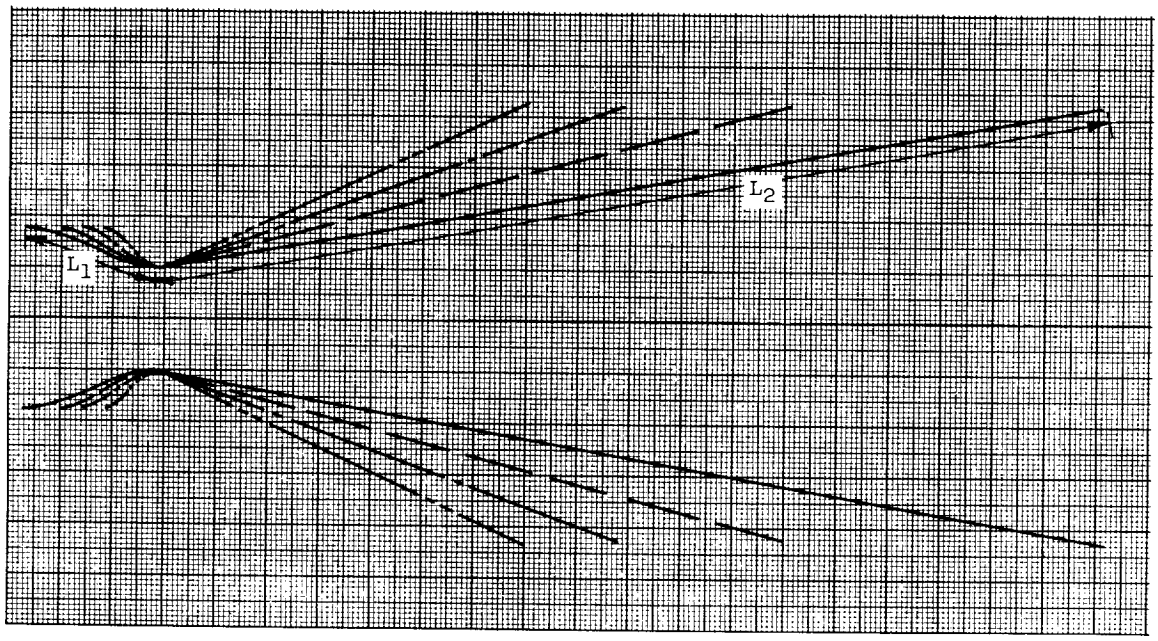

(b) Family of nozzles such that L_2/L_1 = constant.

Figure 1. - Description of nozzles.

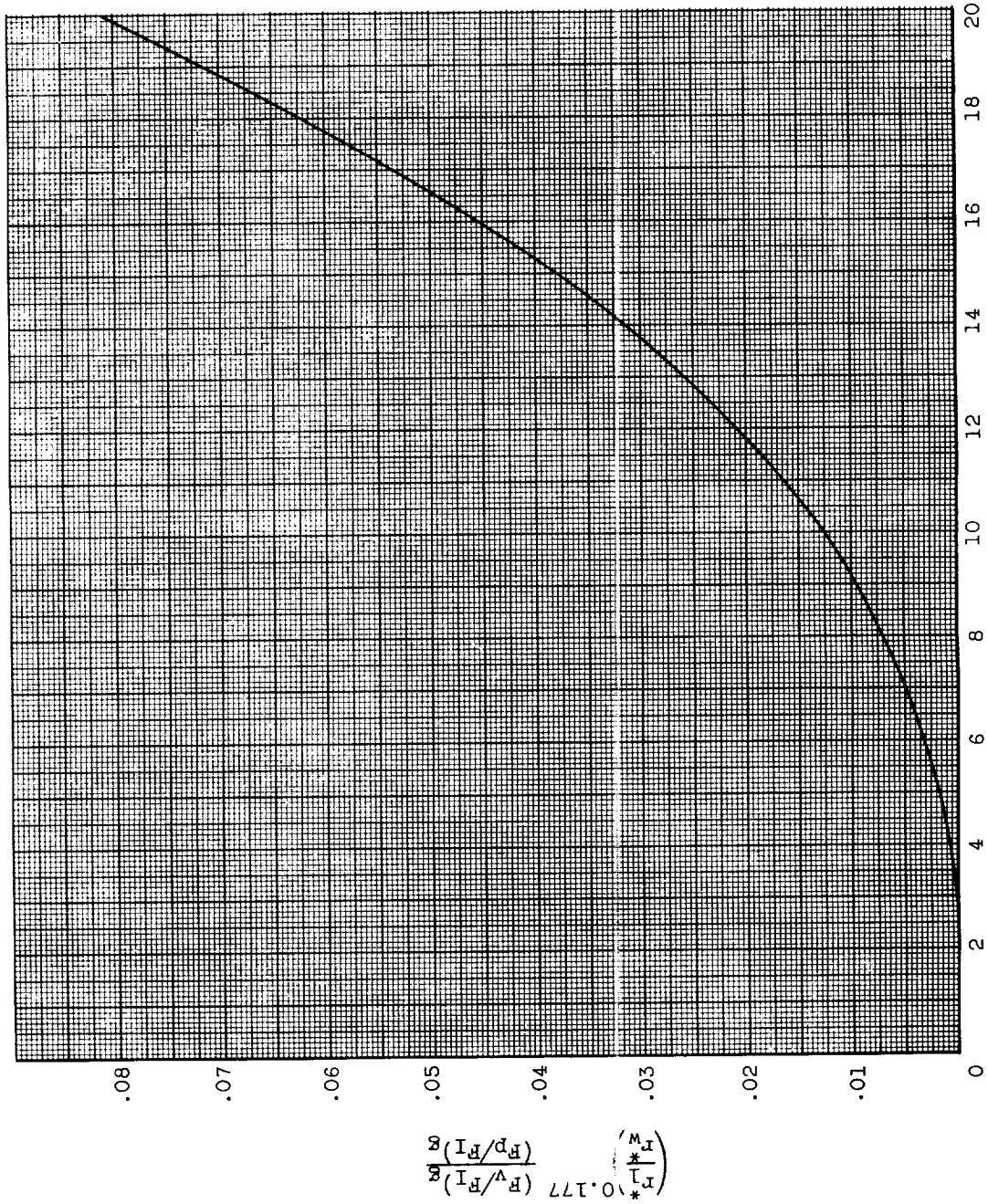

Figure 2. - Plot of equation (13).

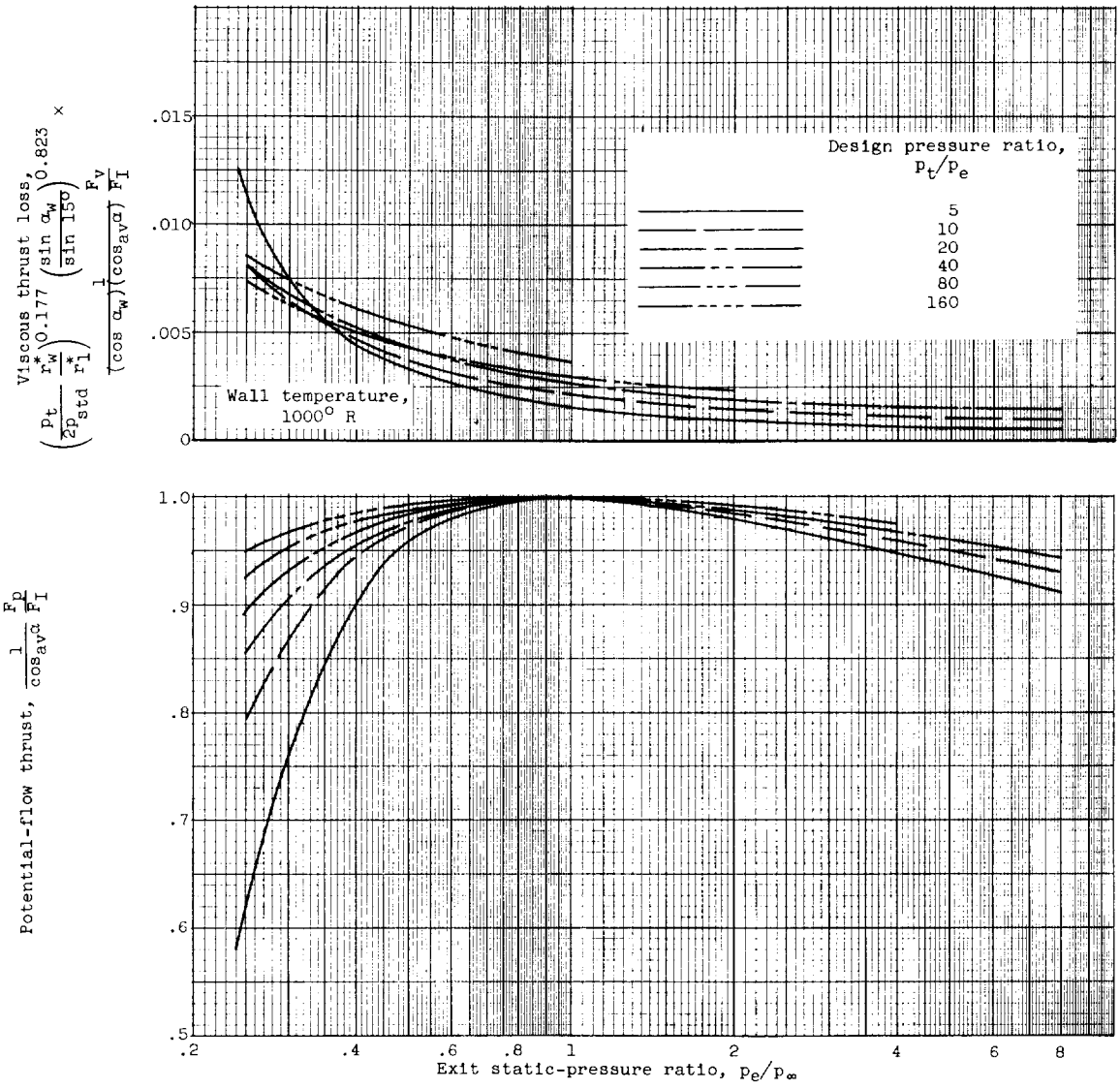

(a) Stagnation temperature, 1000° R.

Figure 3. - Thrust characteristics.

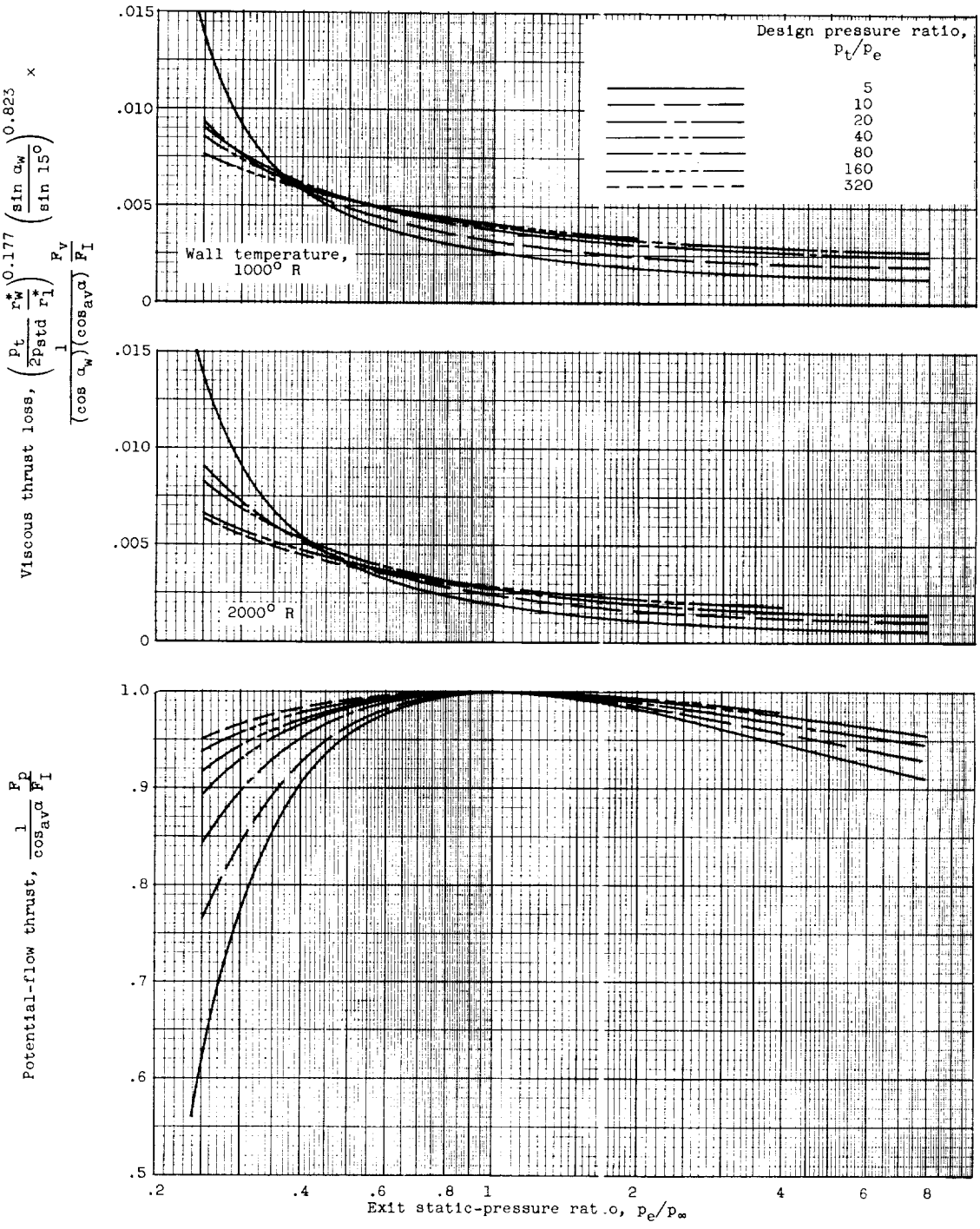

(b) Stagnation temperature, 2000° R.

Figure 3. - Continued. Thrust characteristics.

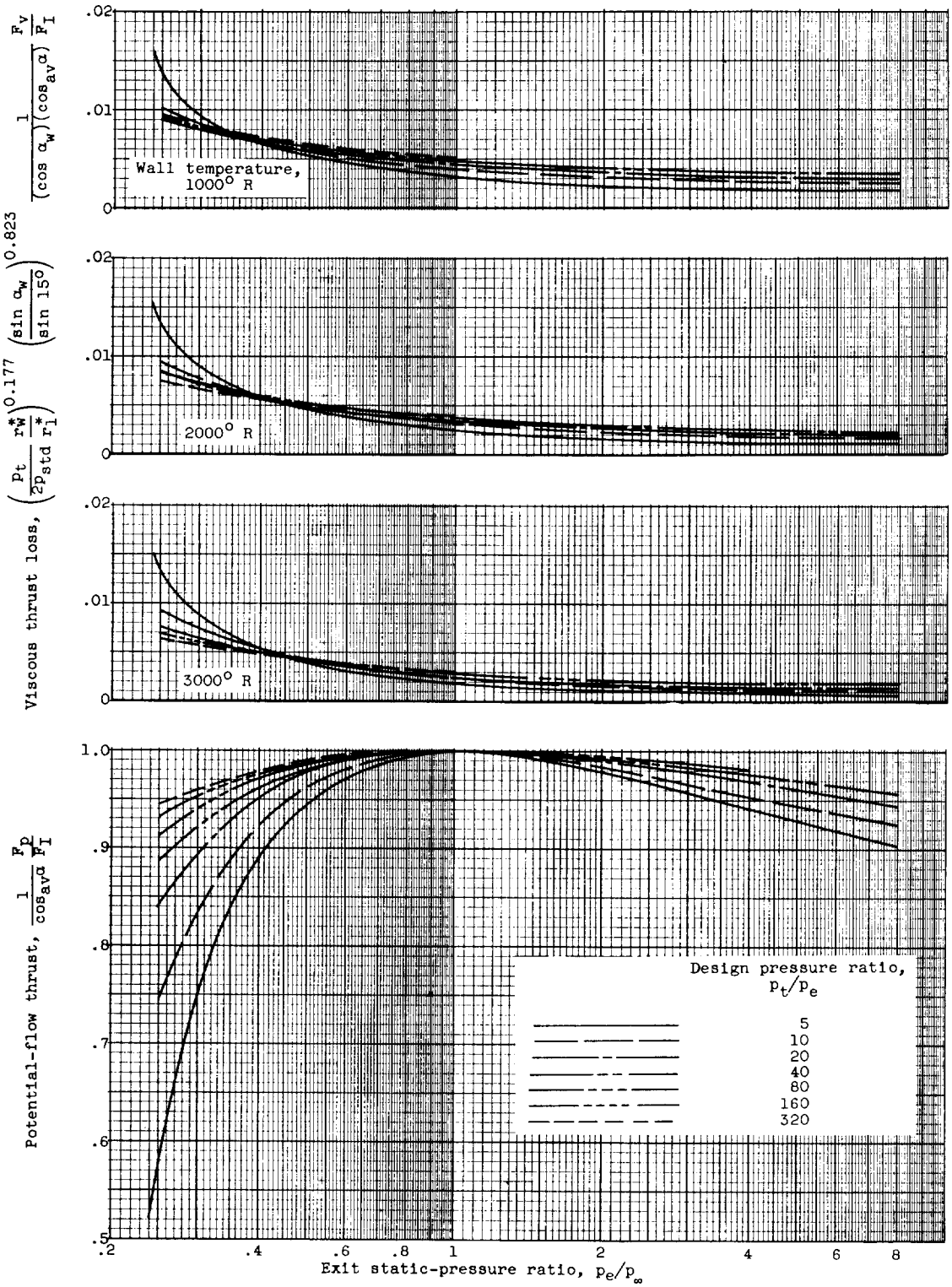

(c) Stagnation temperature, 3000° R.

Figure 3. - Continued. Thrust characteristics.

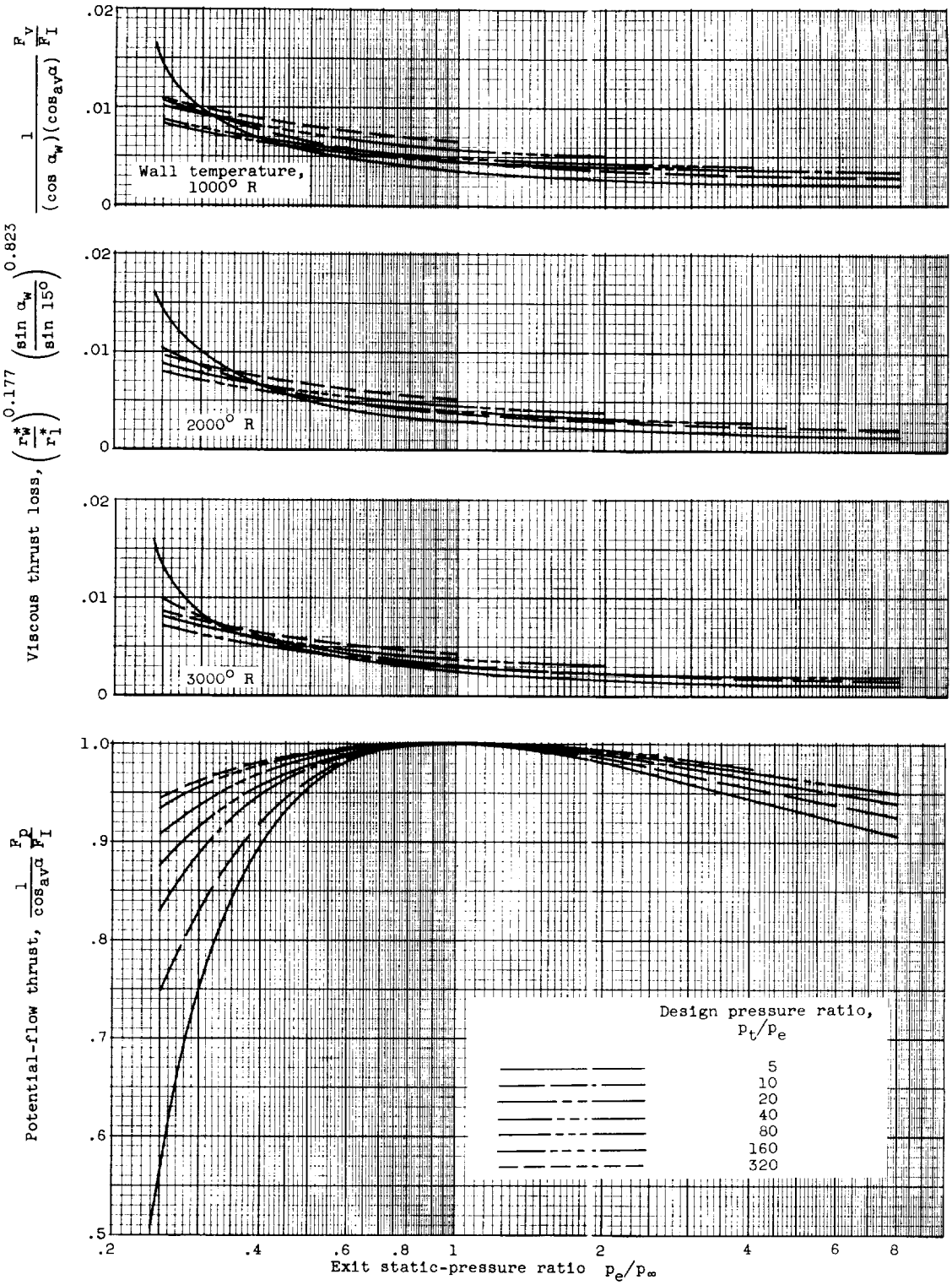

(d) Stagnation temperature, 4000° R; stagnation pressure, $2p_{std}$.

Figure 3. - Continued. Thrust characteristics.

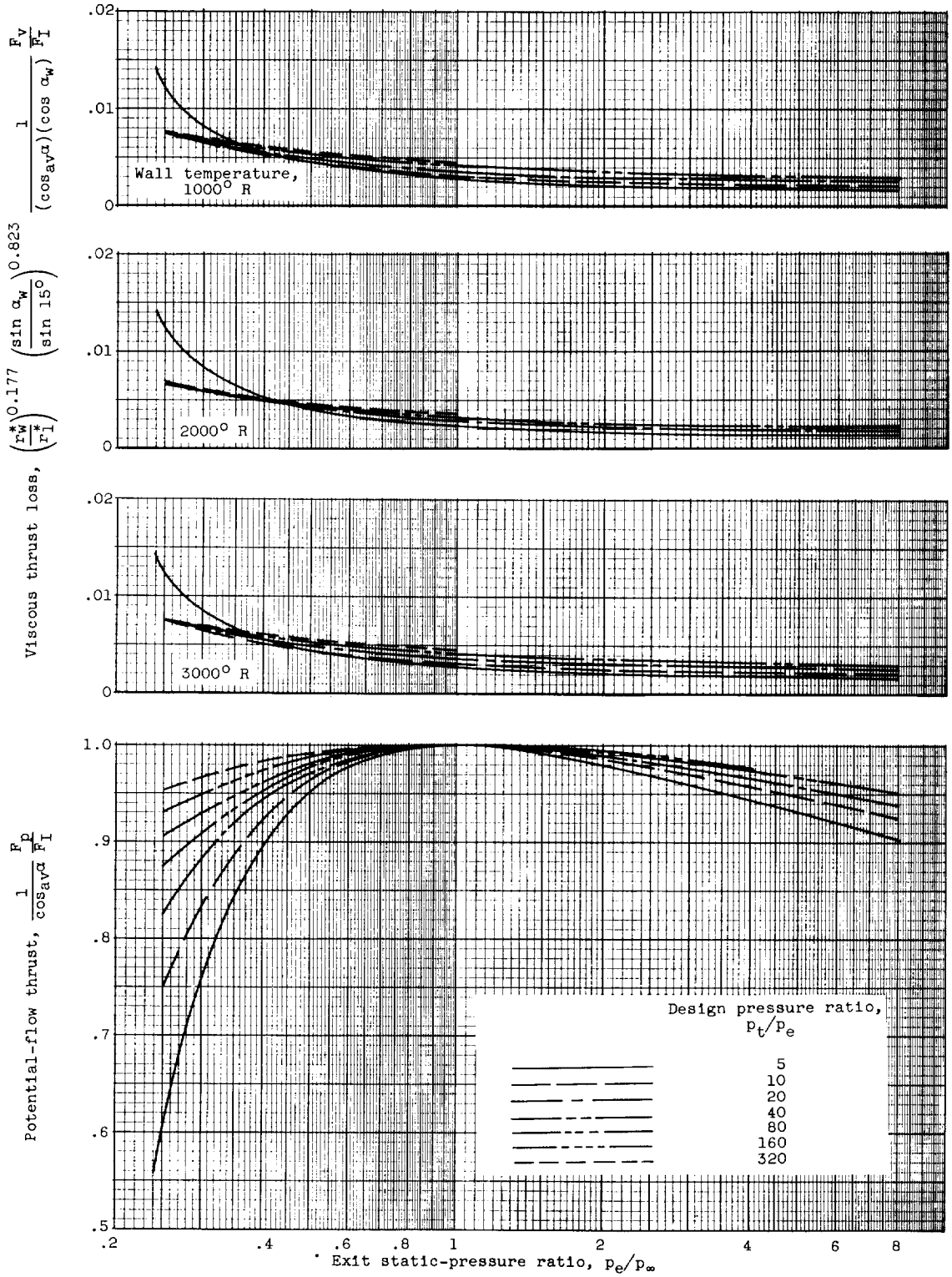

(e) Stagnation temperature, 4000° R; stagnation pressure, $8p_{std}$.

Figure 3. - Continued. Thrust characteristics.

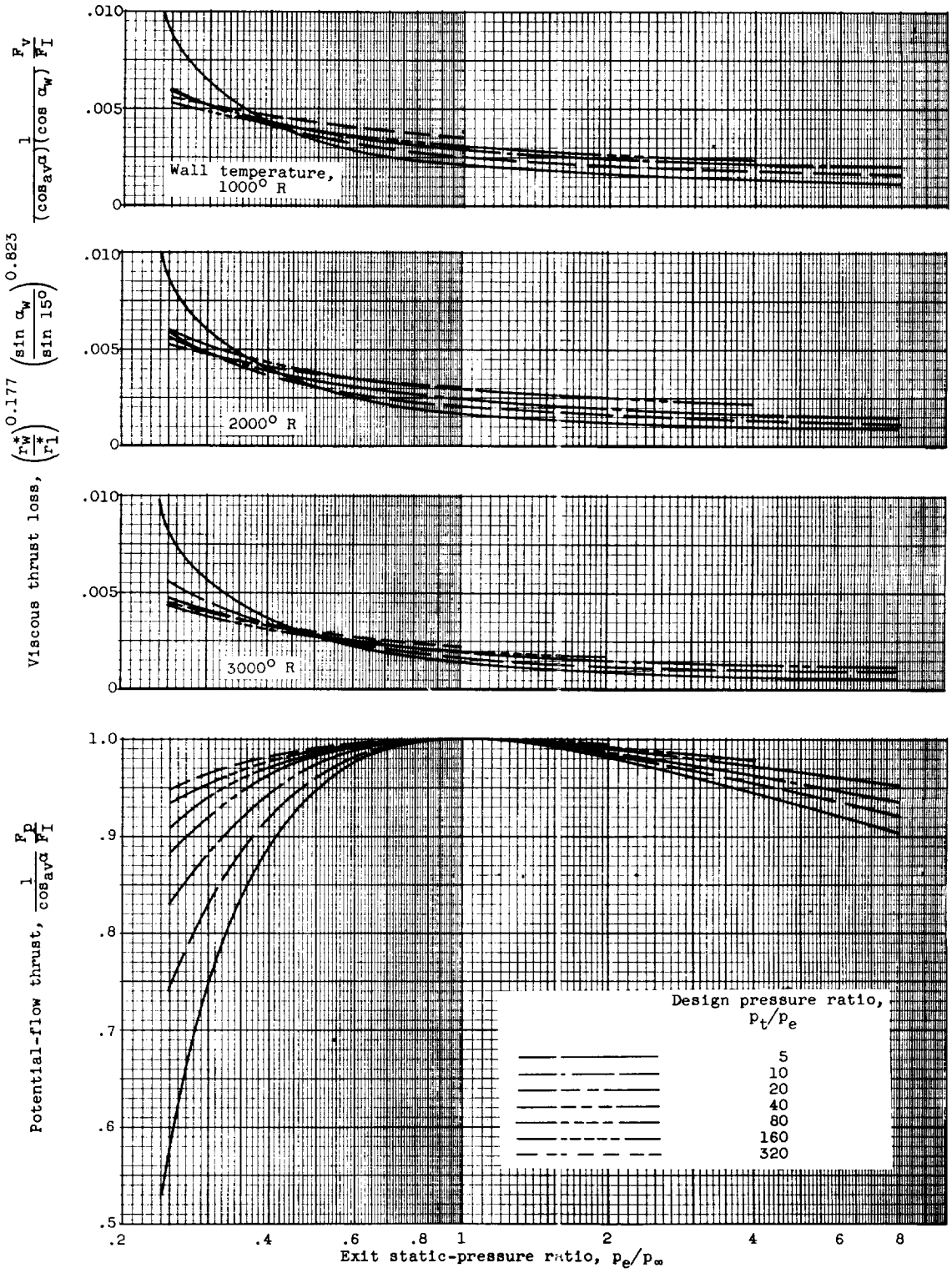

(f) Stagnation temperature, 4000° R; stagnation pressure, $32p_{std}$.

Figure 3. - Continued. Thrust characteristics.

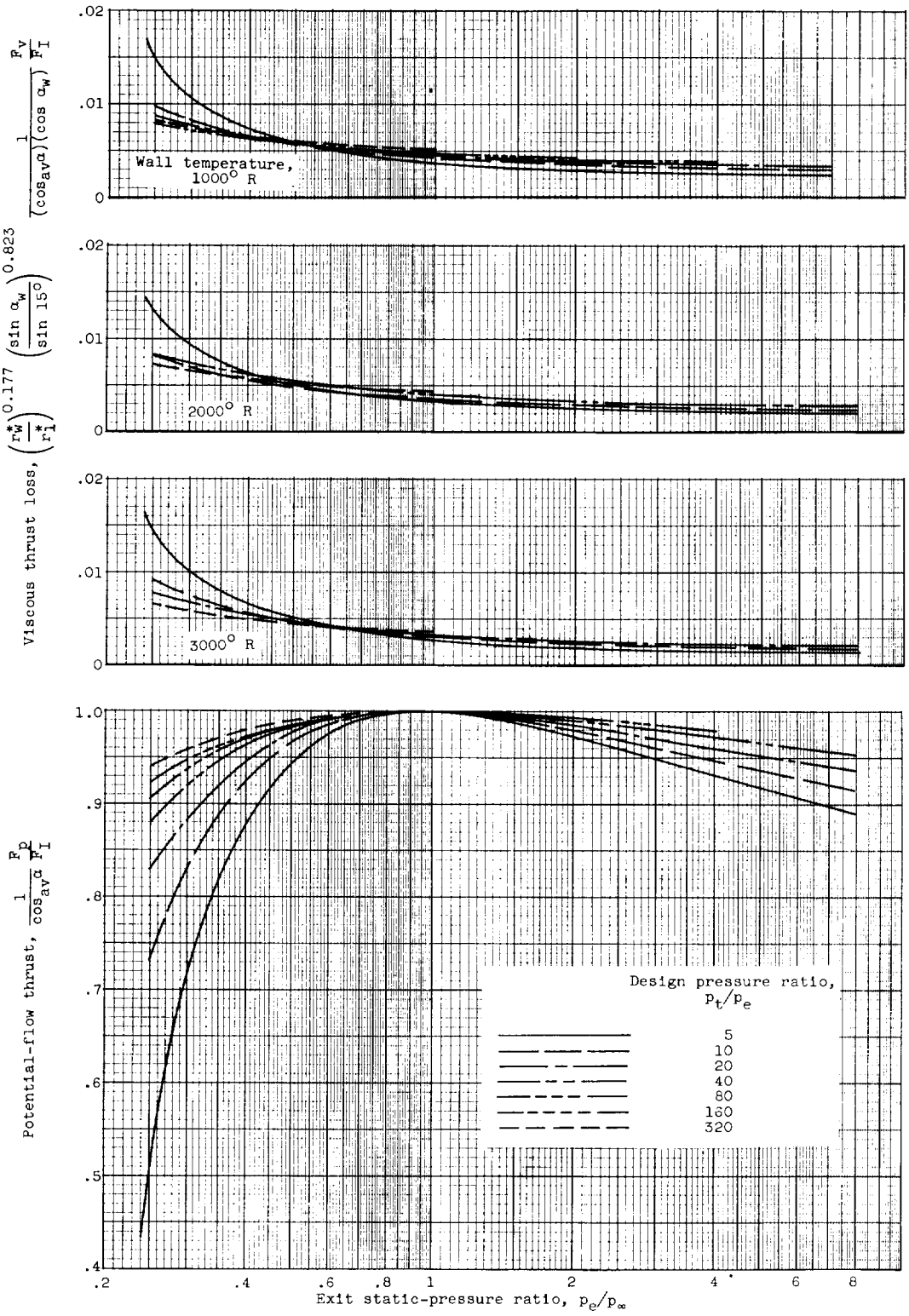

(g) Stagnation temperature, 5000° R; stagnation pressure, $2p_{std}$.

Figure 3. - Continued. Thrust characteristics.

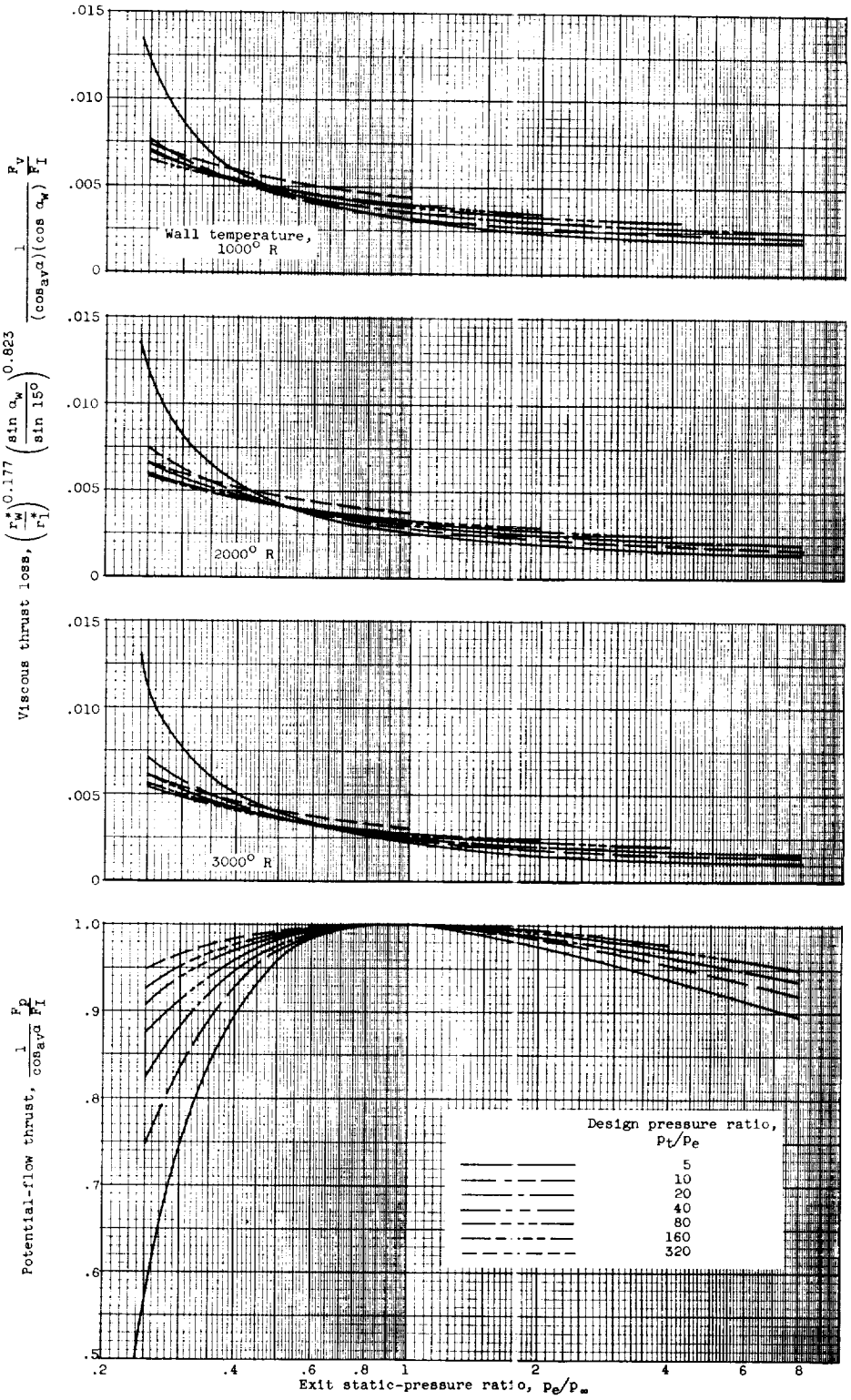

(h) Stagnation temperature, 5000° R; stagnation pressure, $8p_{std}$.

Figure 3. - Continued. Thrust characteristics.

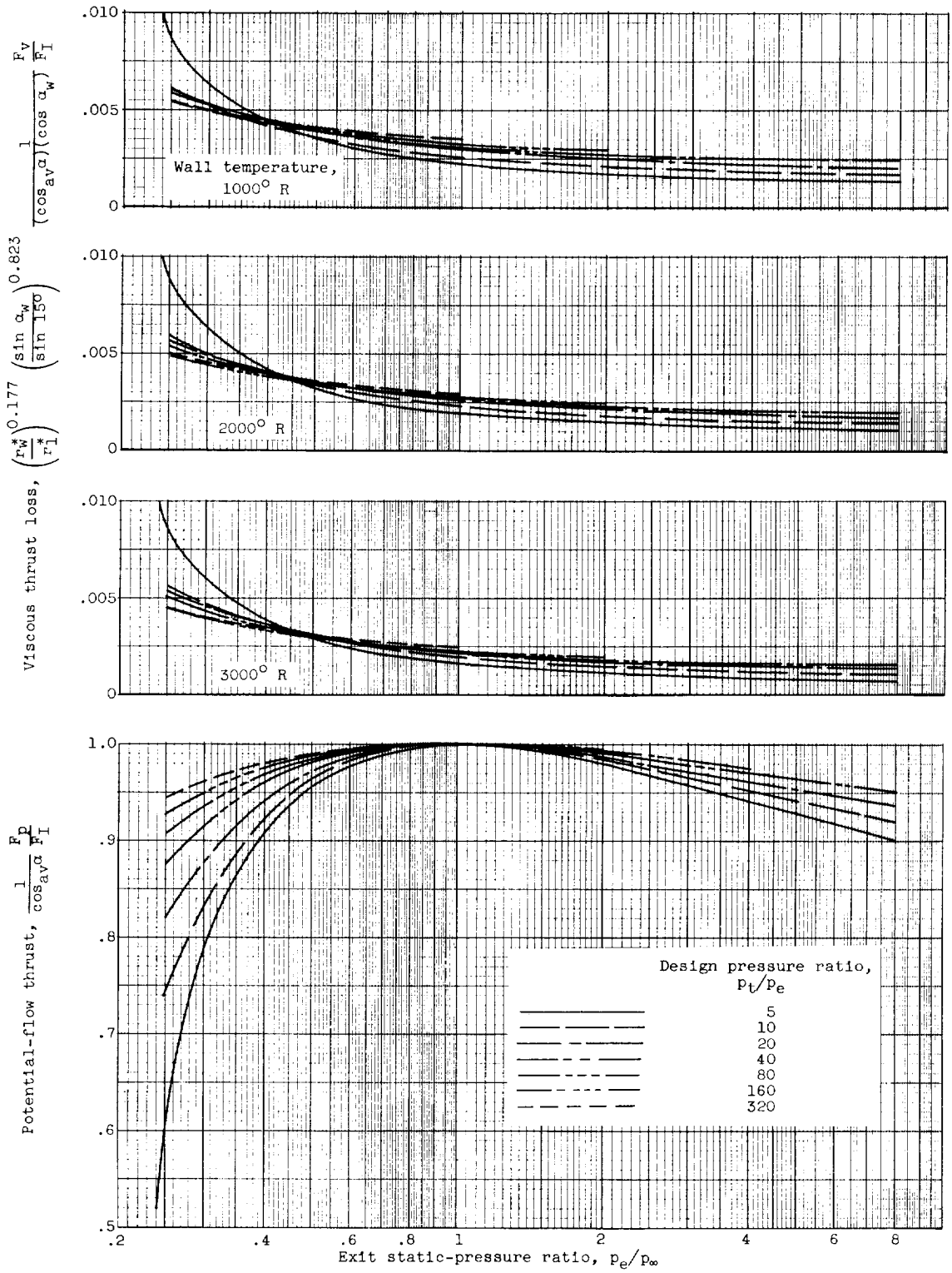

(1) Stagnation temperature, 5000° R; stagnation pressure, $32p_{std}$.

Figure 3. - Continued. Thrust characteristics.

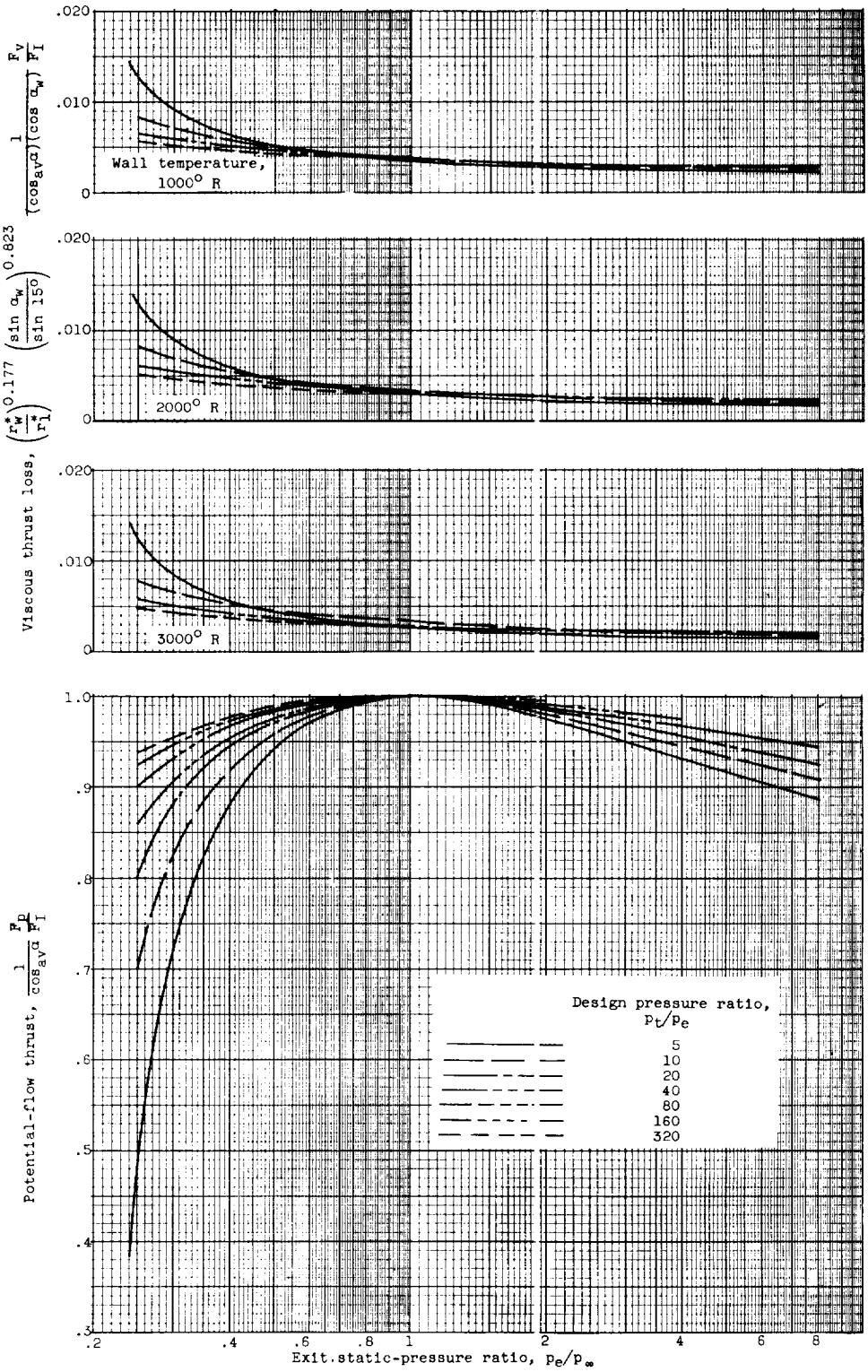

(j) Stagnation temperature, 6000° R; stagnation pressure, $2p_{std}$.

Figure 3. - Continued. Thrust characteristics.

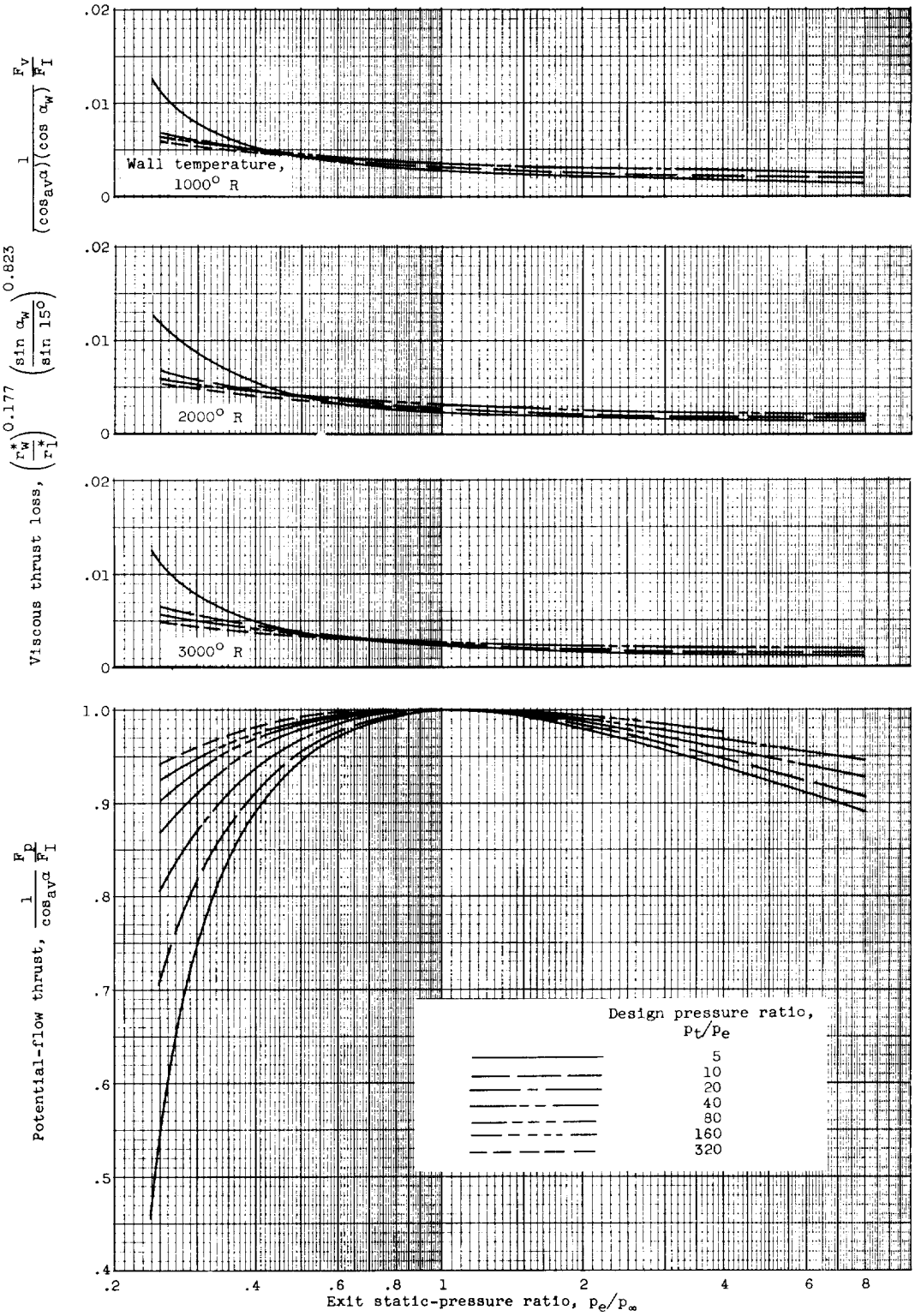

(k) Stagnation temperature, 6000° R; stagnation pressure, $8p_{std}$.

Figure 3. - Continued. Thrust characteristics.

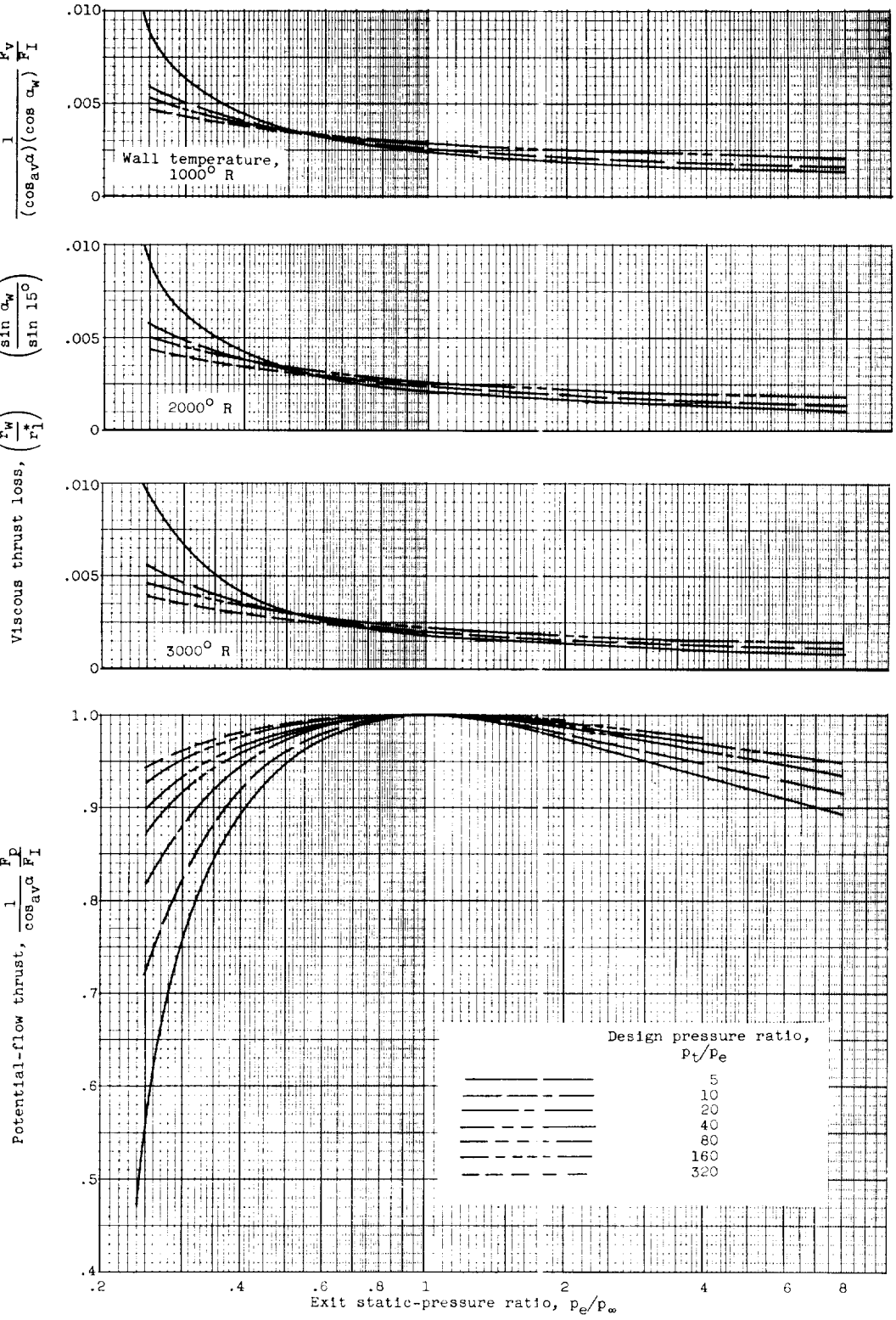

(l) Stagnation temperature, 6000° R; stagnation pressure, $32p_{std}$.

Figure 3. - Concluded. Thrust characteristics.

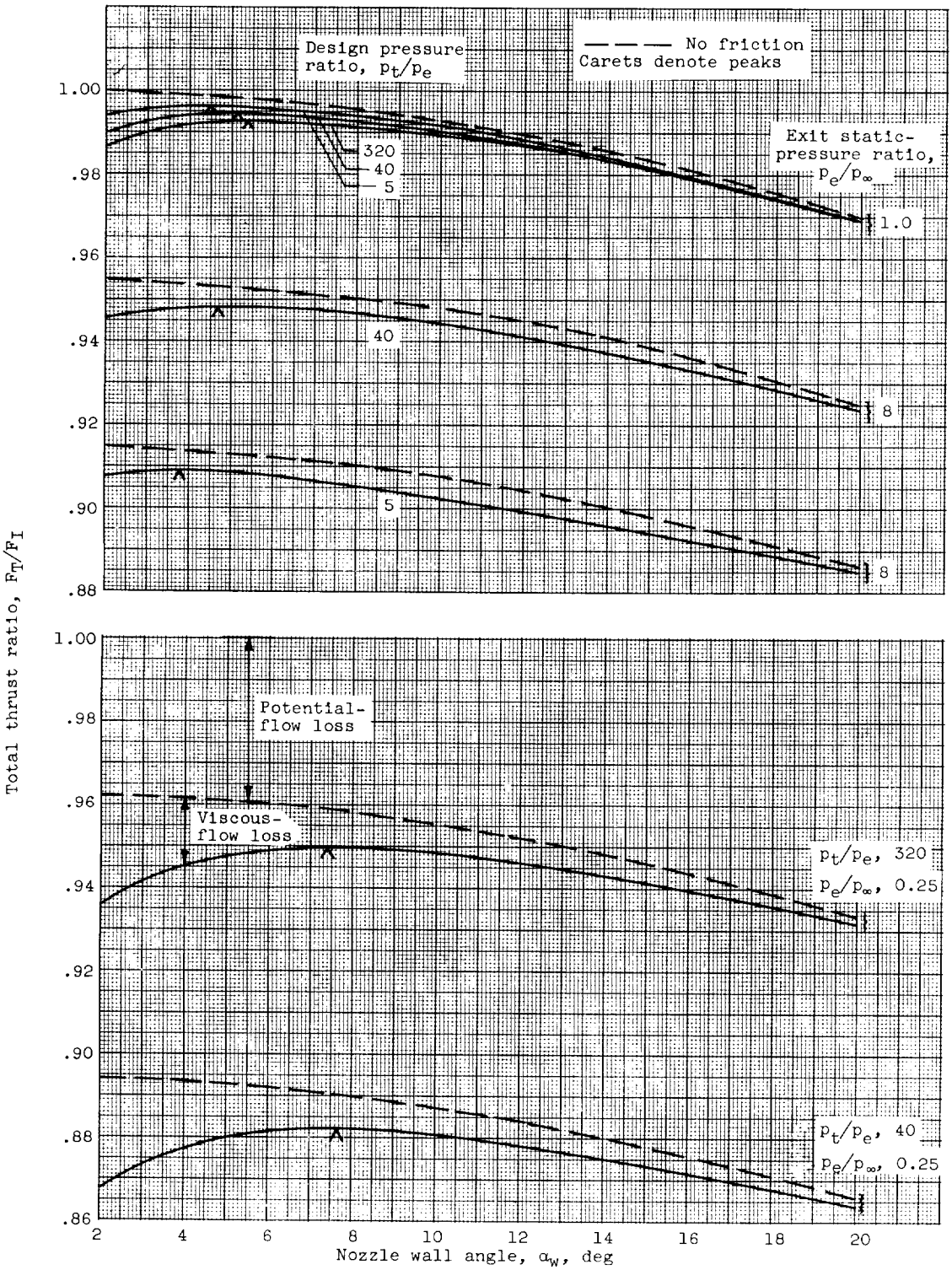

(a) Variation with exit static-pressure ratio and design pressure ratio. T_w, 1000° R; T_t, 1000° R; p_t/p_{std}, 32; r_w^*, 1.

Figure 4. - Effect of nozzle wall angle on total thrust ratio.

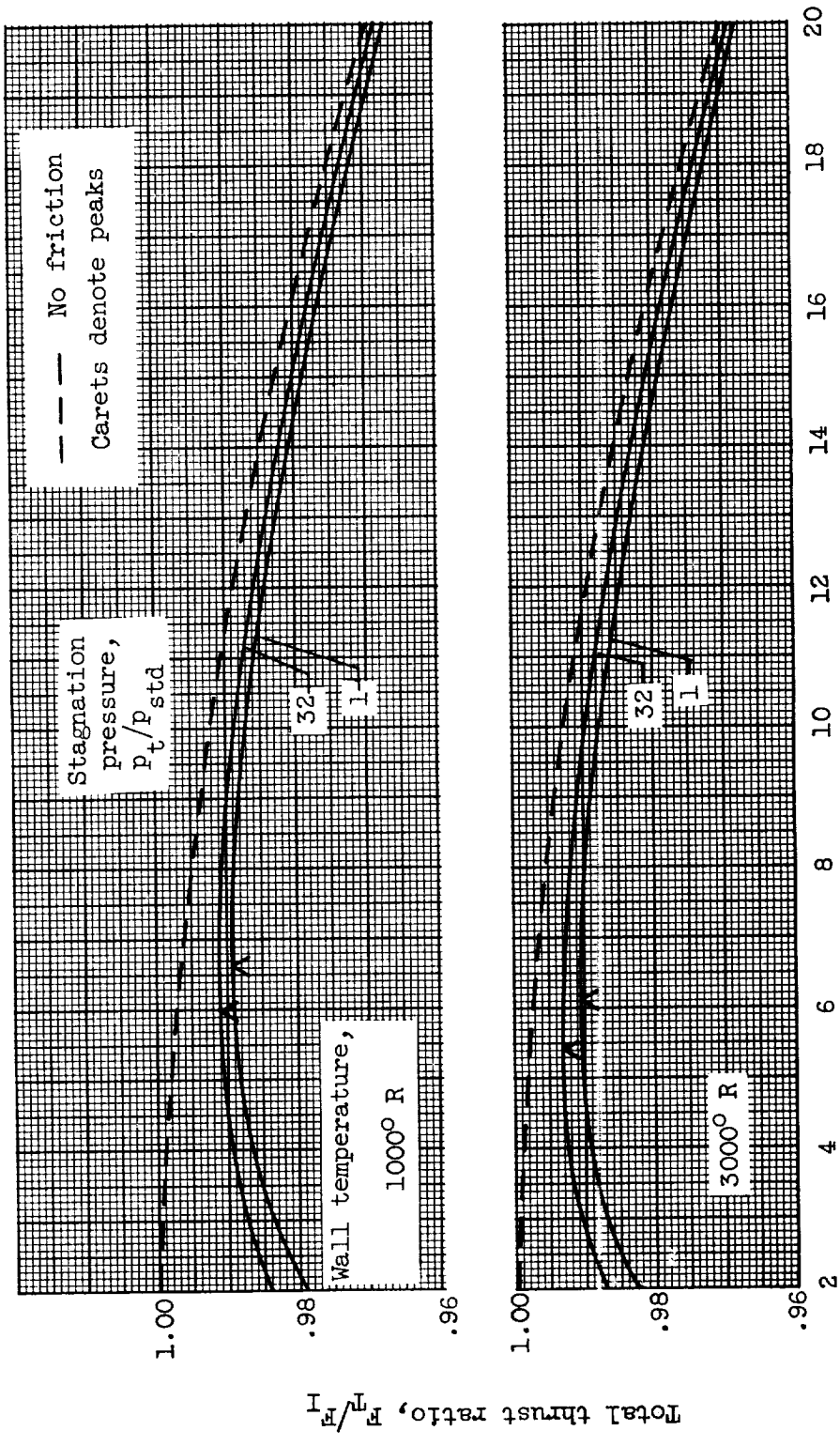

(b) Variation with stagnation pressure and wall temperature. T_t, 6000° R; p_t/p_e, 40; p_e/p_∞, 1; r_w^*, 1.

Figure 4. - Concluded. Effect of nozzle wall angle on total thrust ratio.

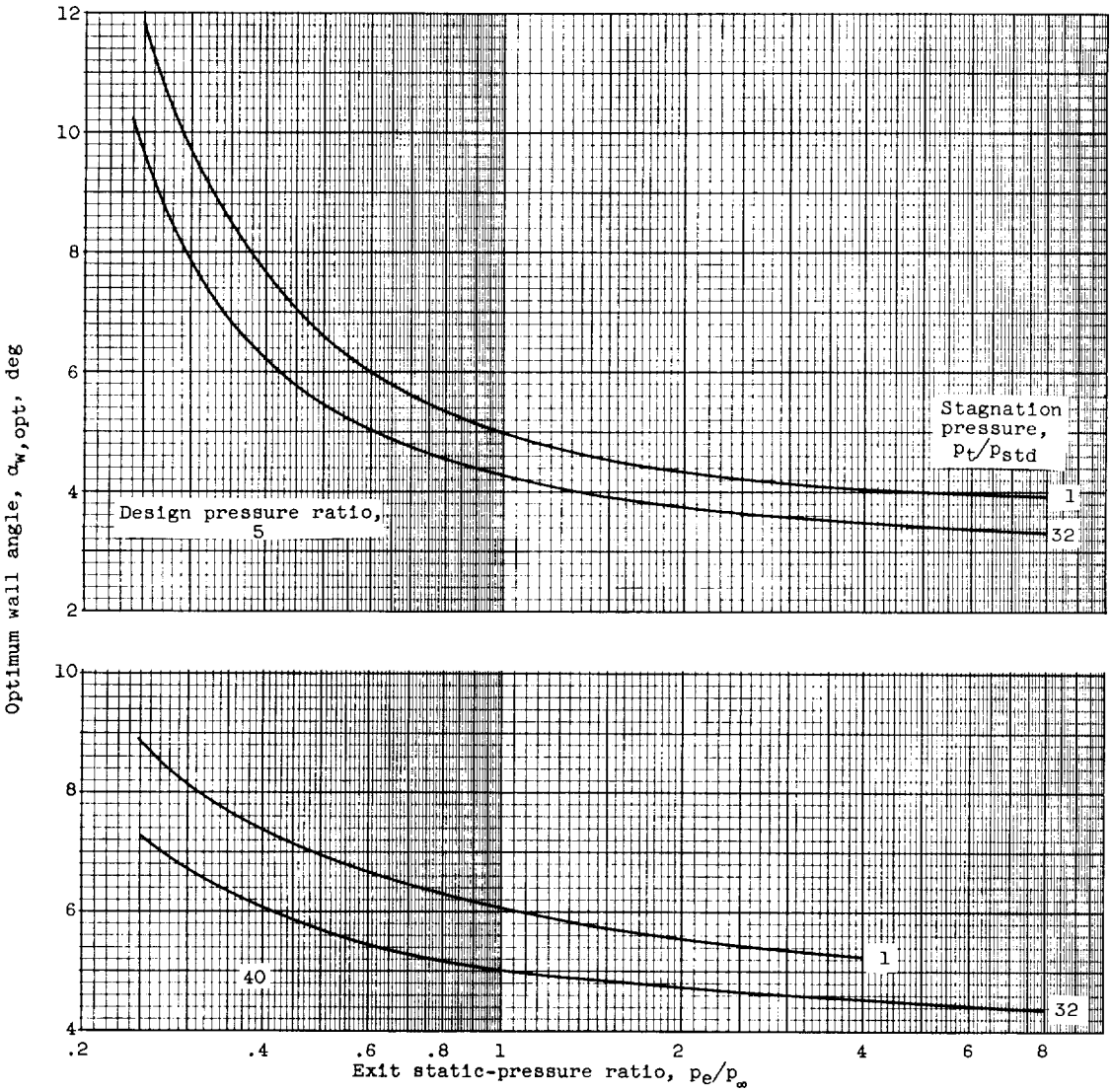

(a) Variation with potential-stream stagnation pressure and exit static-pressure ratio. T_w, 1000° R; T_t, 1000° R; r_w^*, 1.

Figure 5. - Optimum nozzle wall angle.

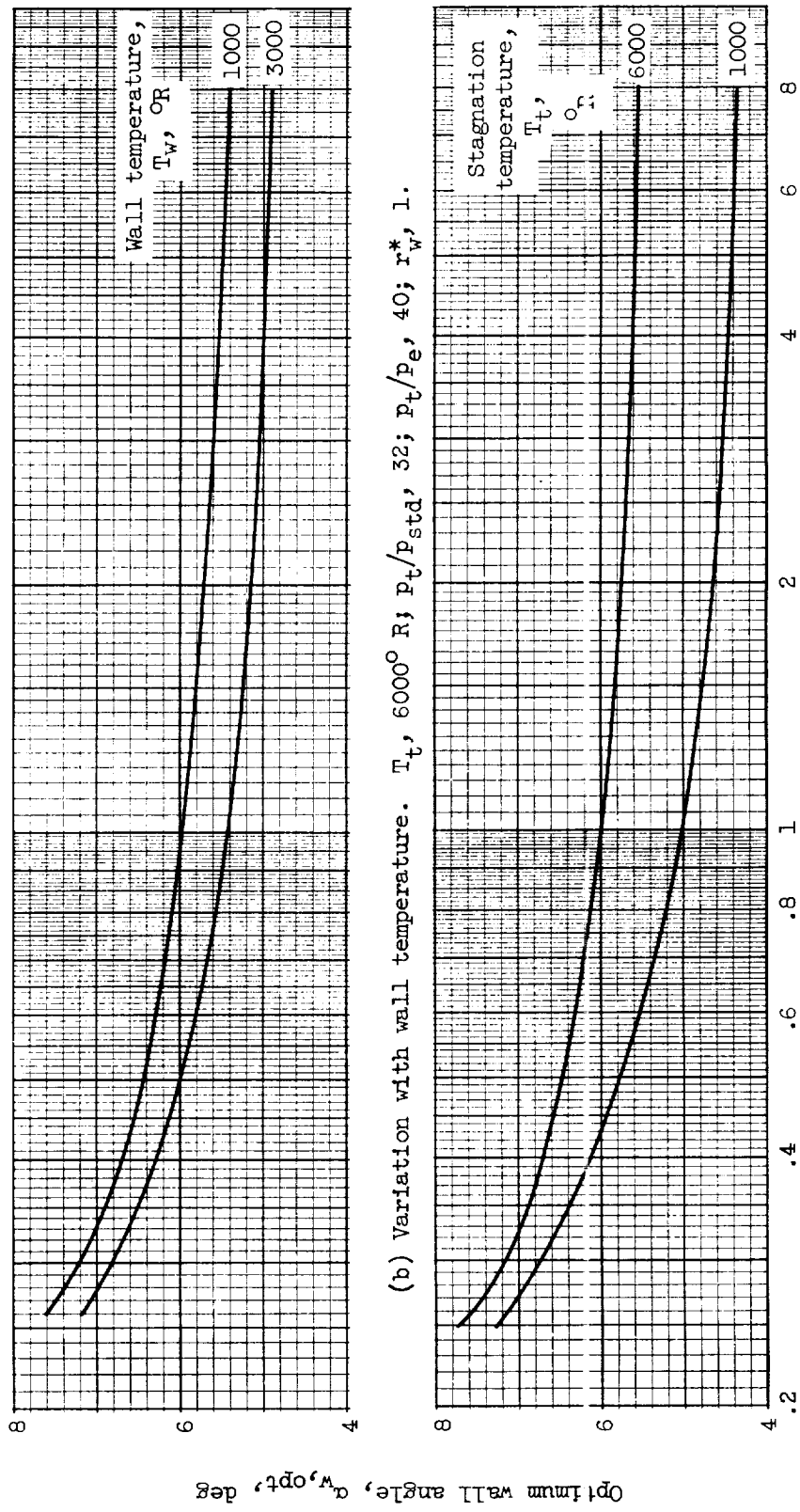

(b) Variation with wall temperature. T_t, 6000° R; p_t/p_{std}, 32; p_t/p_e, 40; r_w^*, 1.

(c) Variation with potential-stream stagnation temperature. p_t/p_e, 40; T_w, 1000° R; p_t/p_{std}, 32; r_w^*, 1.

Figure 5. - Concluded. Optimum nozzle wall angle.

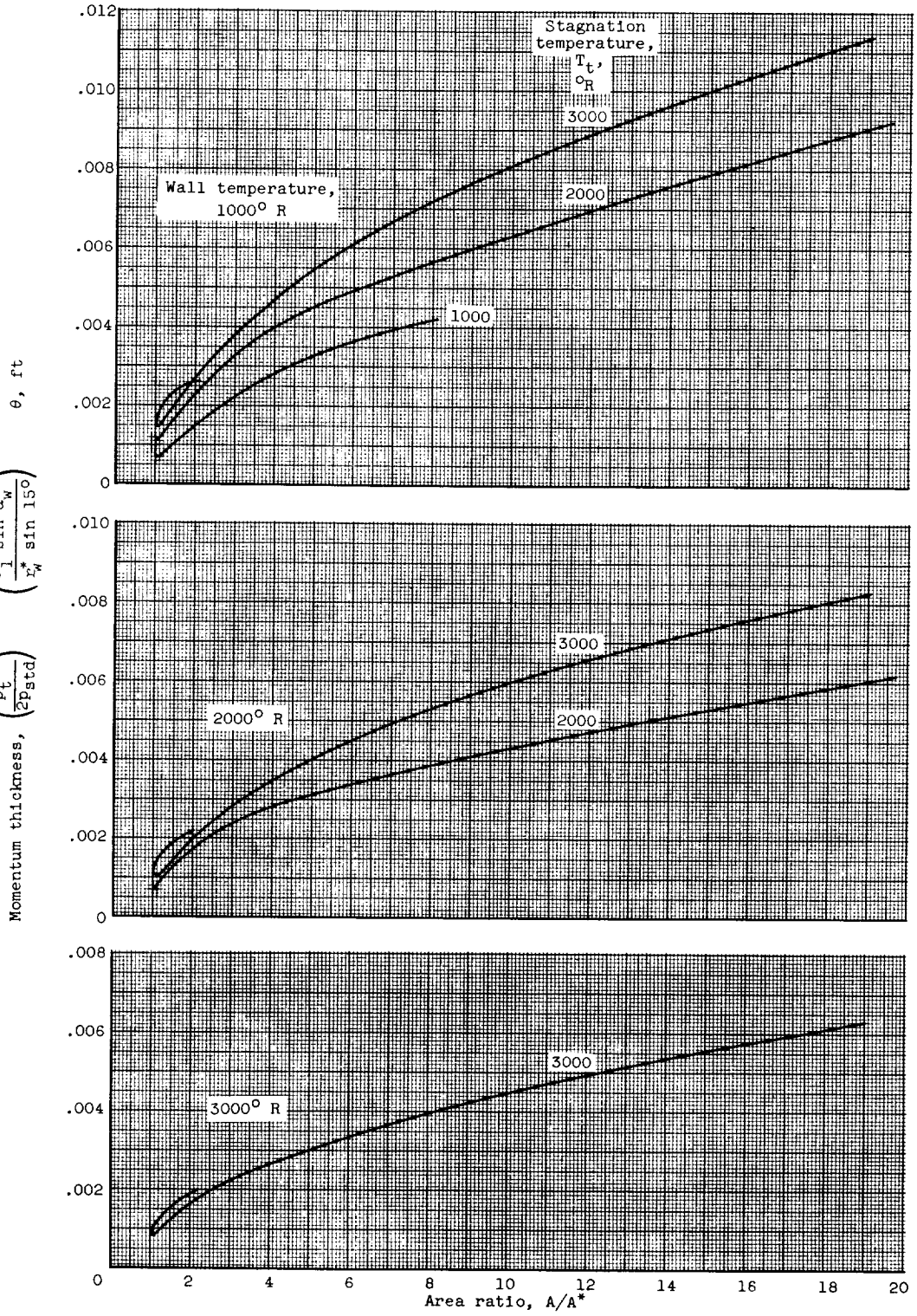

(a) Effect of stagnation temperature. Stagnation pressure, $2p_{std}$.

Figure 6. - Momentum thickness.

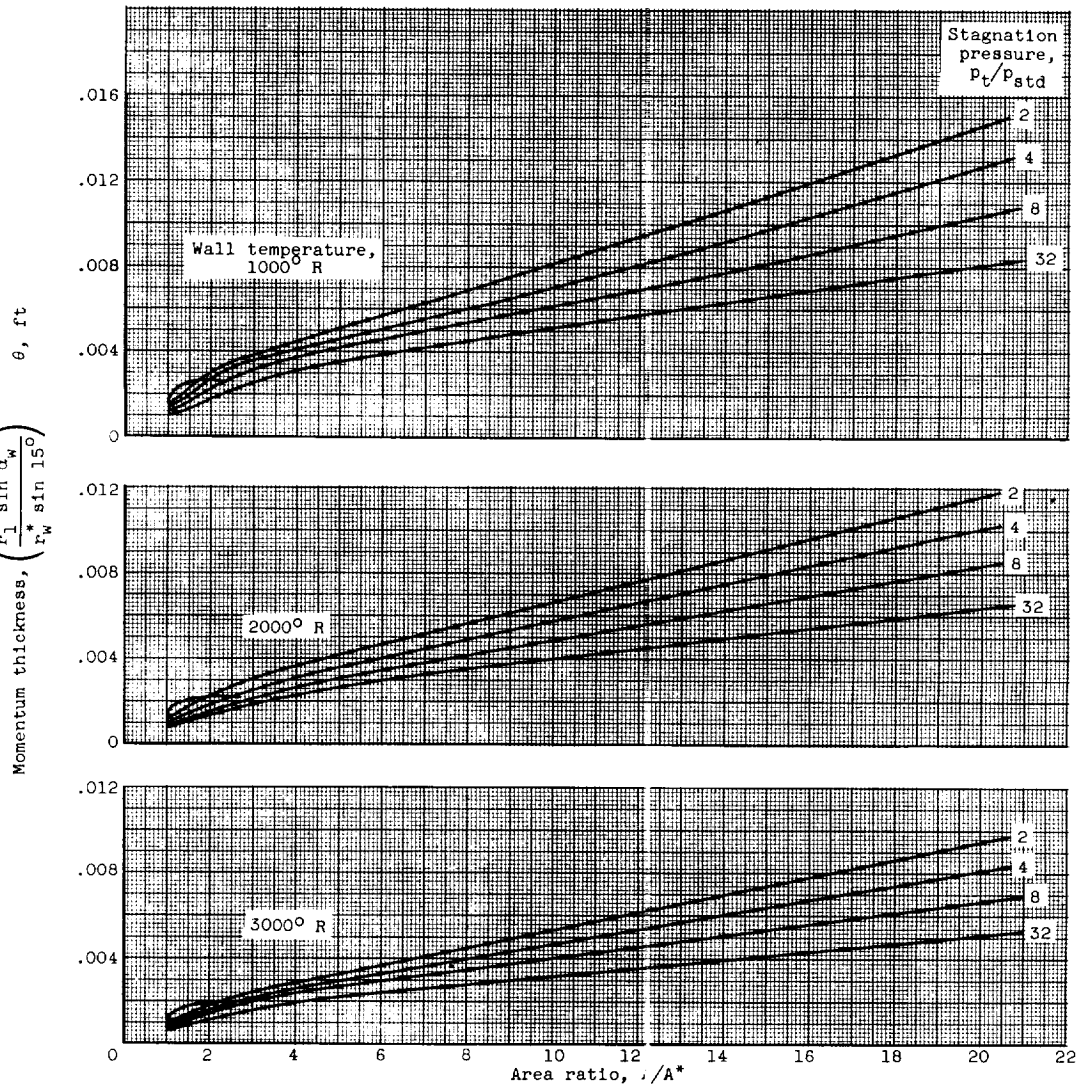

(b) Effect of stagnation pressure. Stagnation temperature, 4000° R.

Figure 6. - Continued. Momentum thickness.

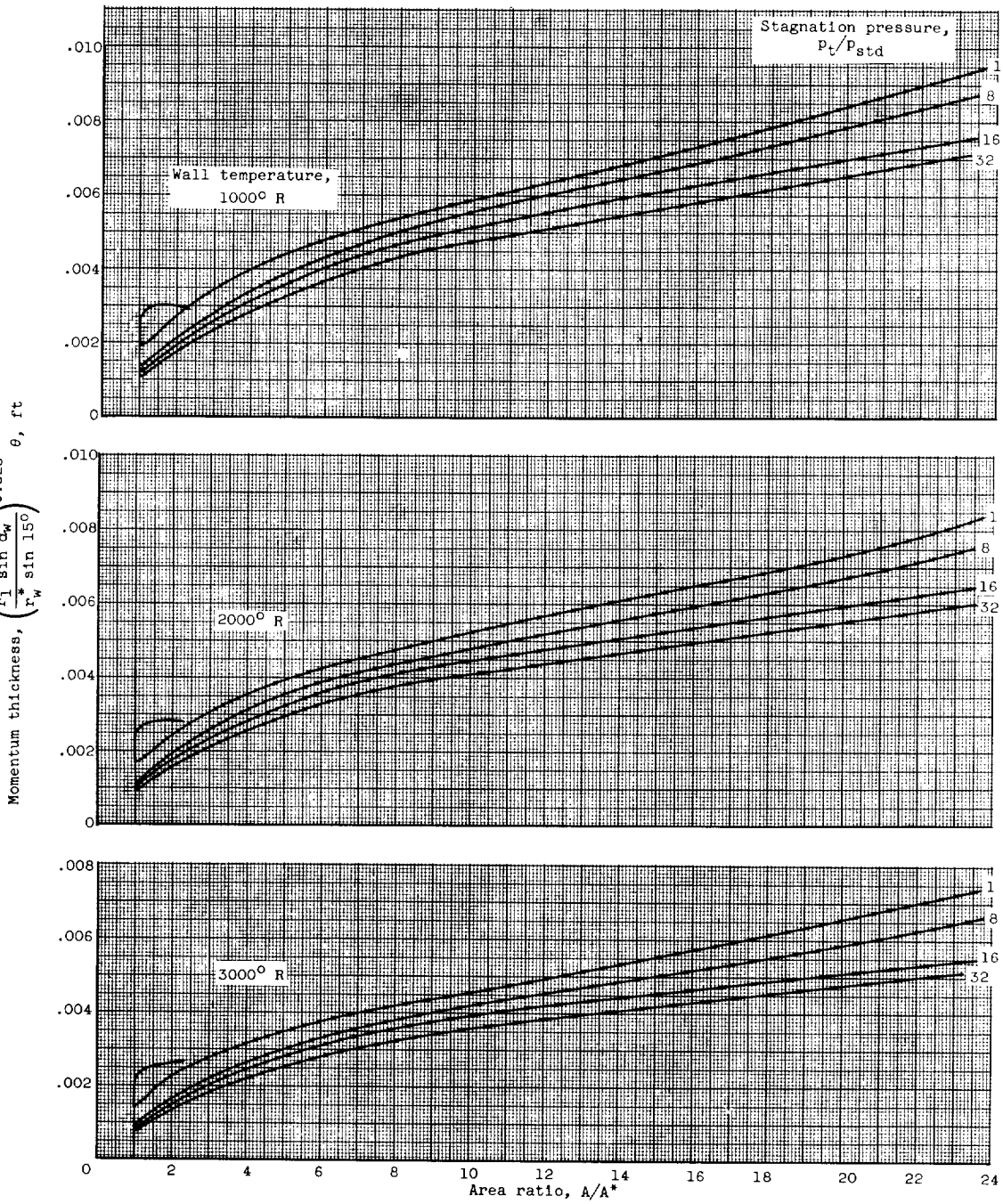

(c) Effect of stagnation pressure. Stagnation temperature, 6000° R.

Figure 6. - Concluded. Momentum thickness.

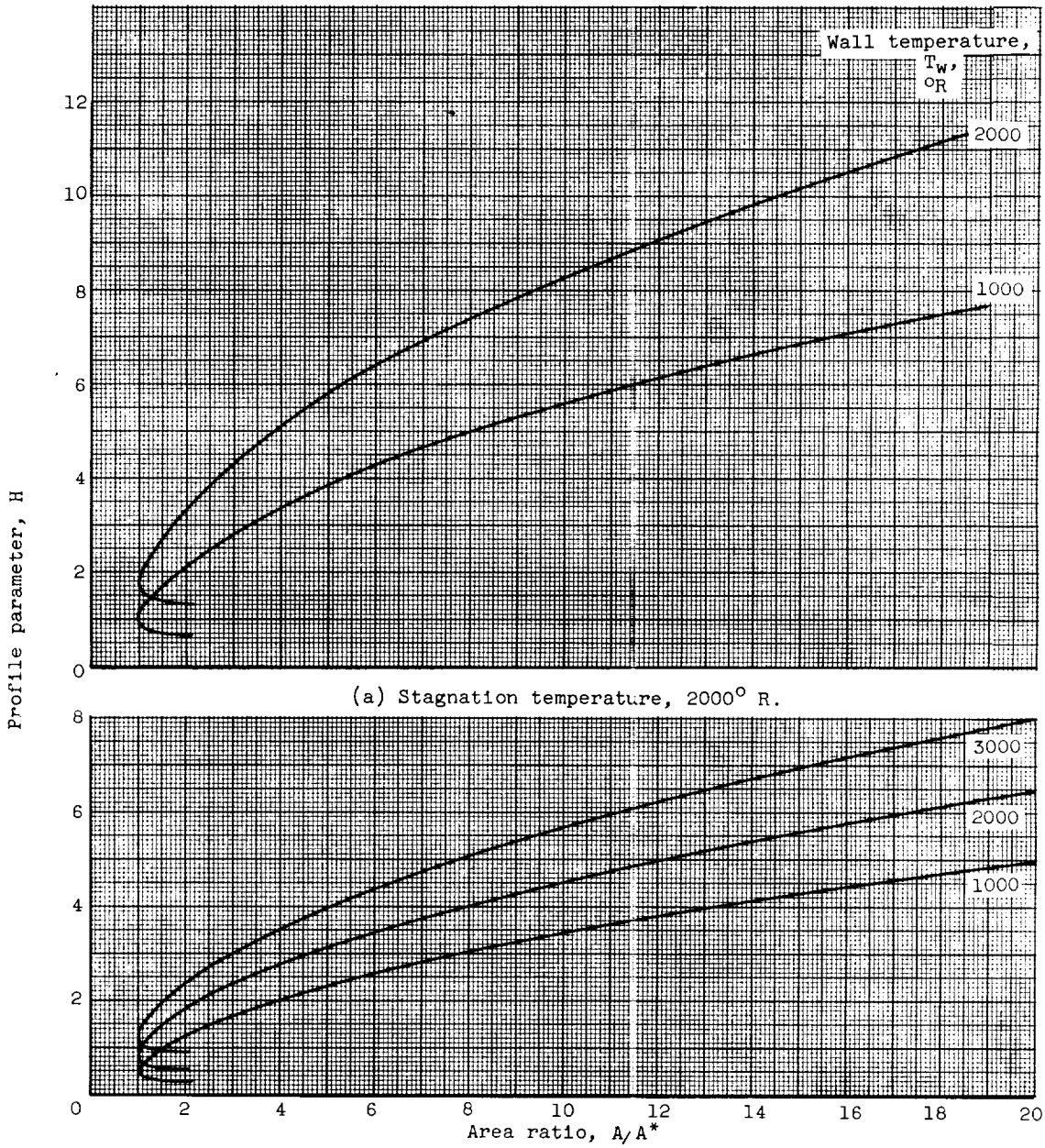

(a) Stagnation temperature, 2000° R.

(b) Stagnation temperature, 4000° R.

Figure 7. - Boundary-layer profiles.

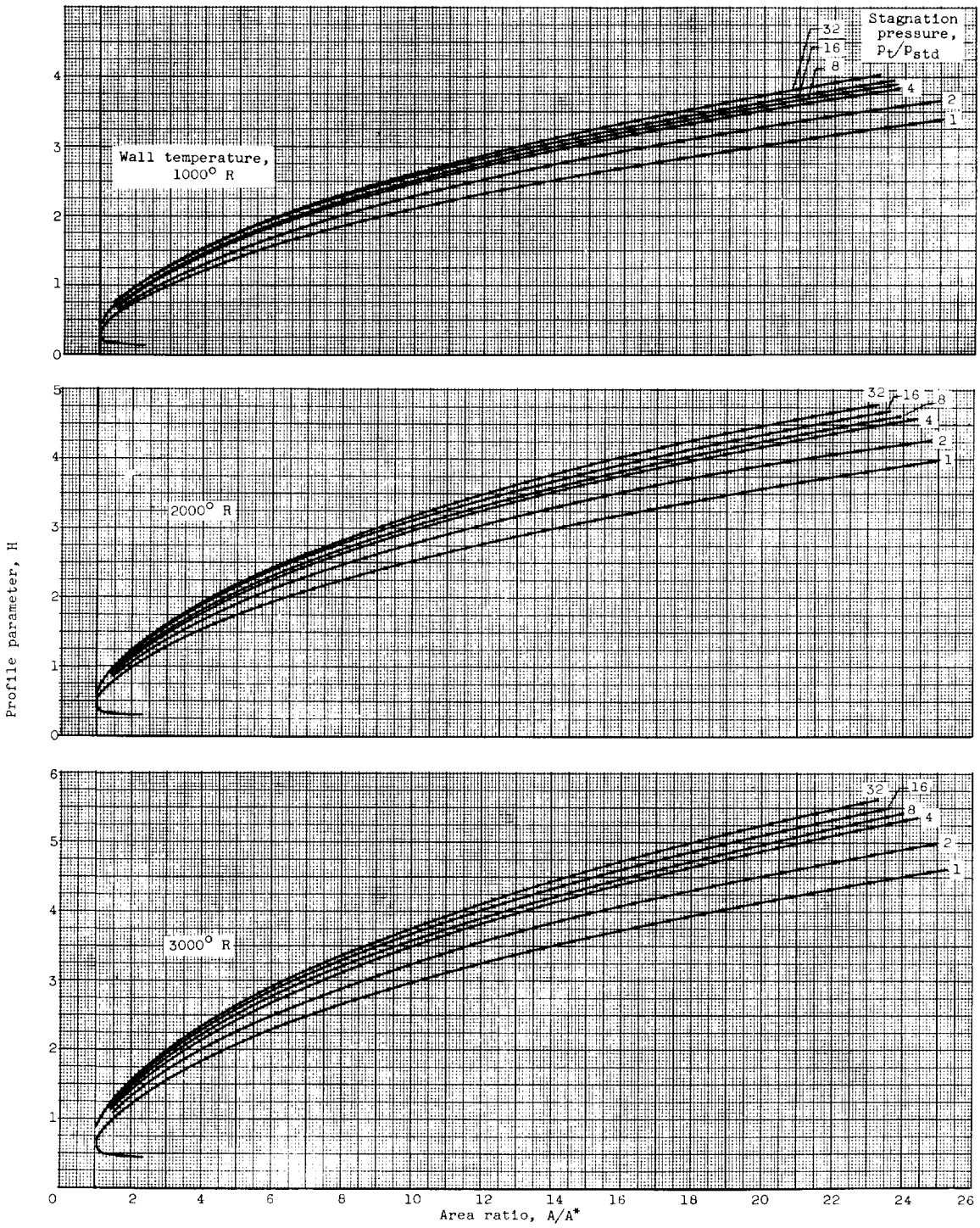

(c) Stagnation temperature, 6000° R.

Figure 7. - Concluded. Boundary-layer profiles.

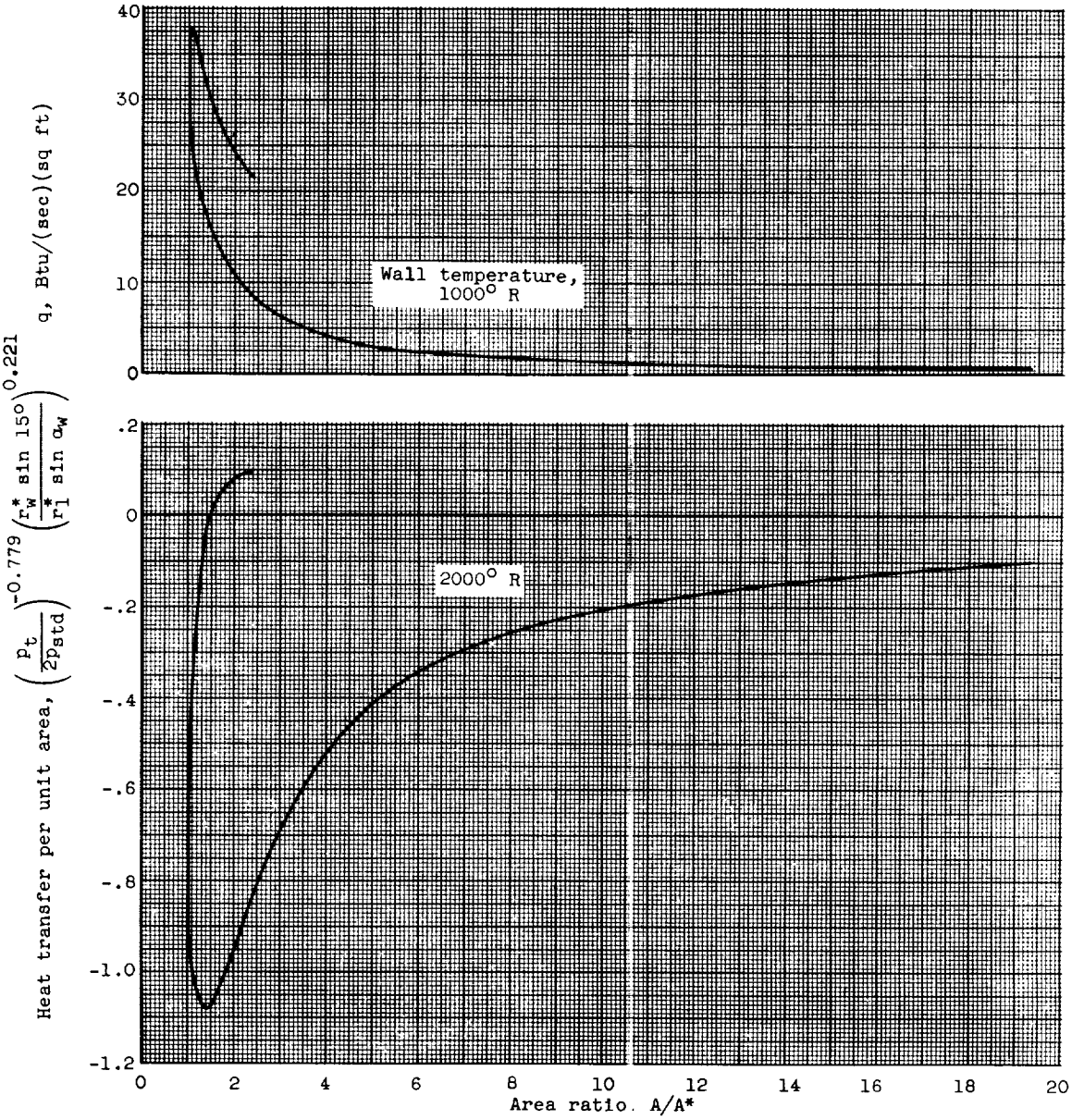

(a) Stagnation temperature, 2000° R.

Figure 8. - Local heat-transfer rate.

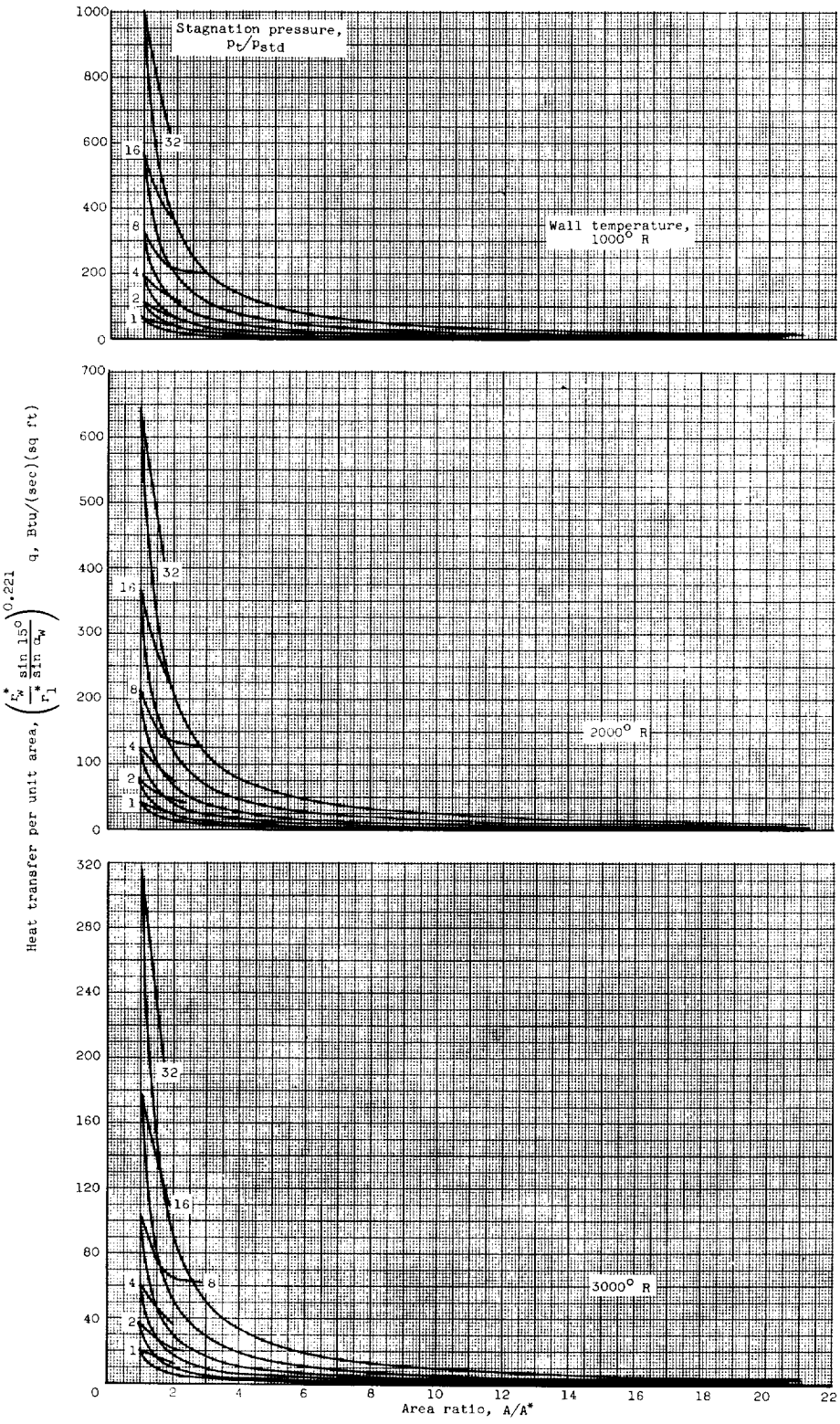

(b) Stagnation temperature, 4000° R.

Figure 8. - Continued. Local heat-transfer rate.

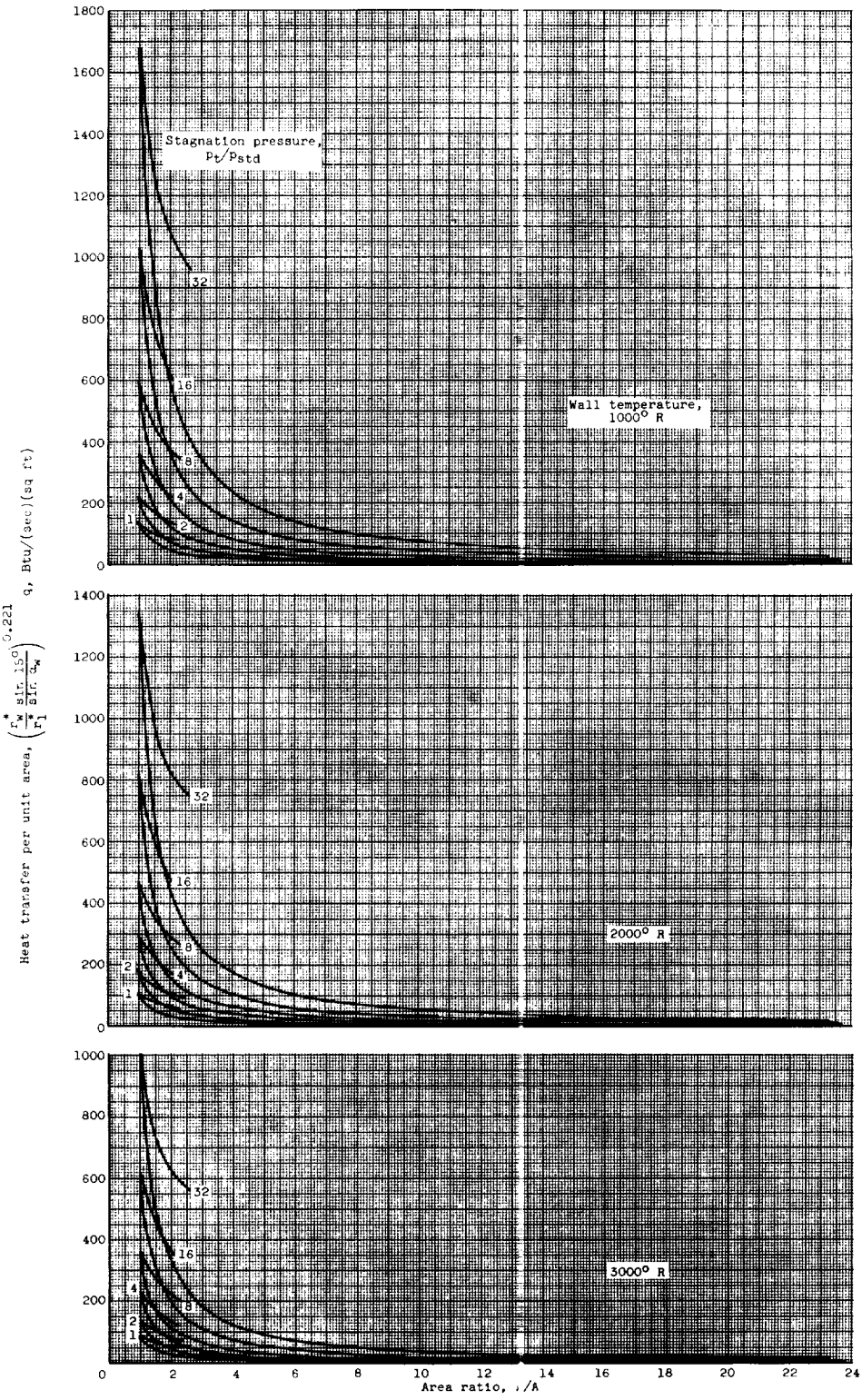

(c) Stagnation temperature, 6000° R.

Figure 8. - Concluded. Local heat-transfer rate.

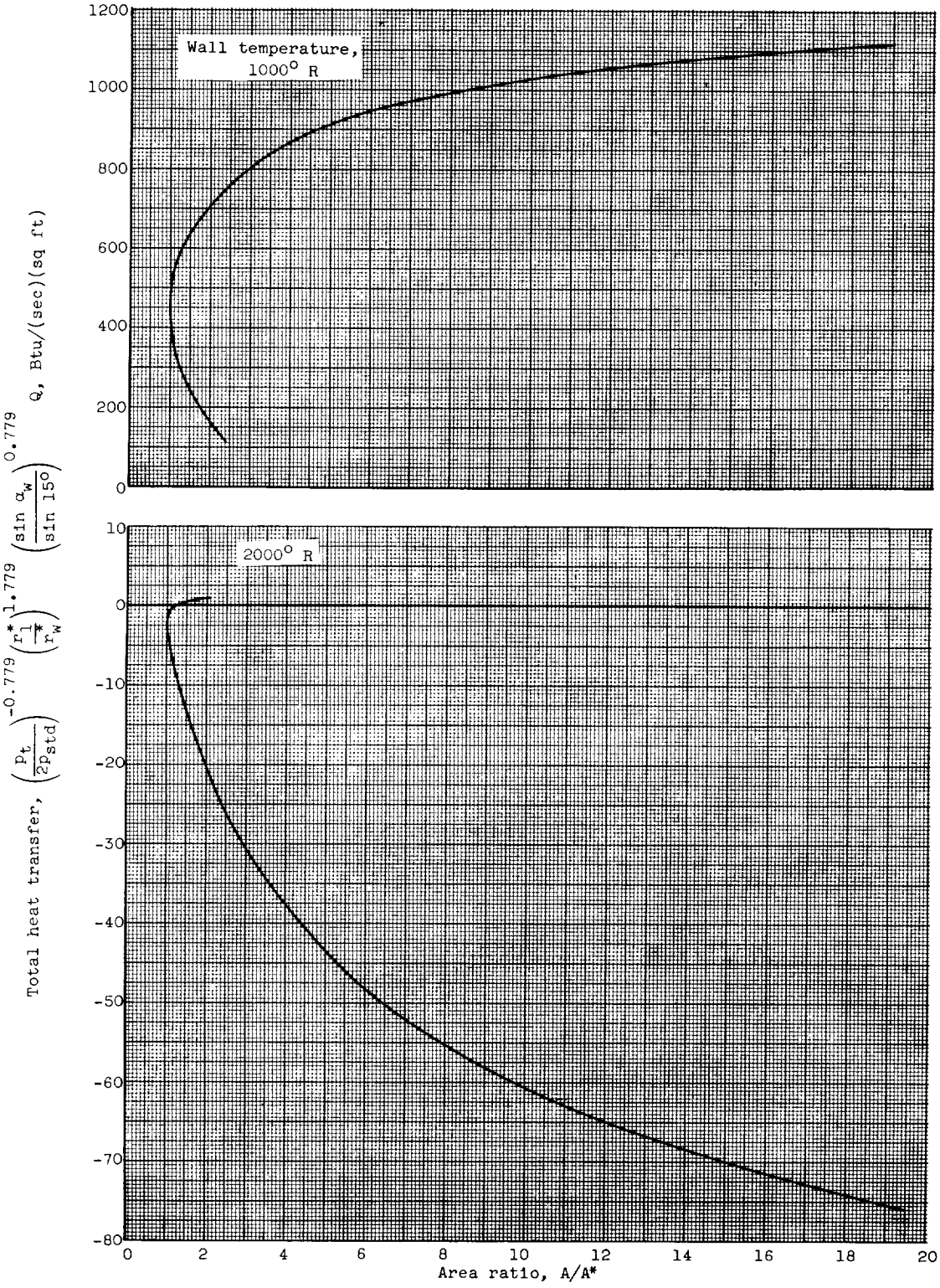

(a) Stagnation temperature, 2000° R.

Figure 9. - Total heat transfer through nozzle.

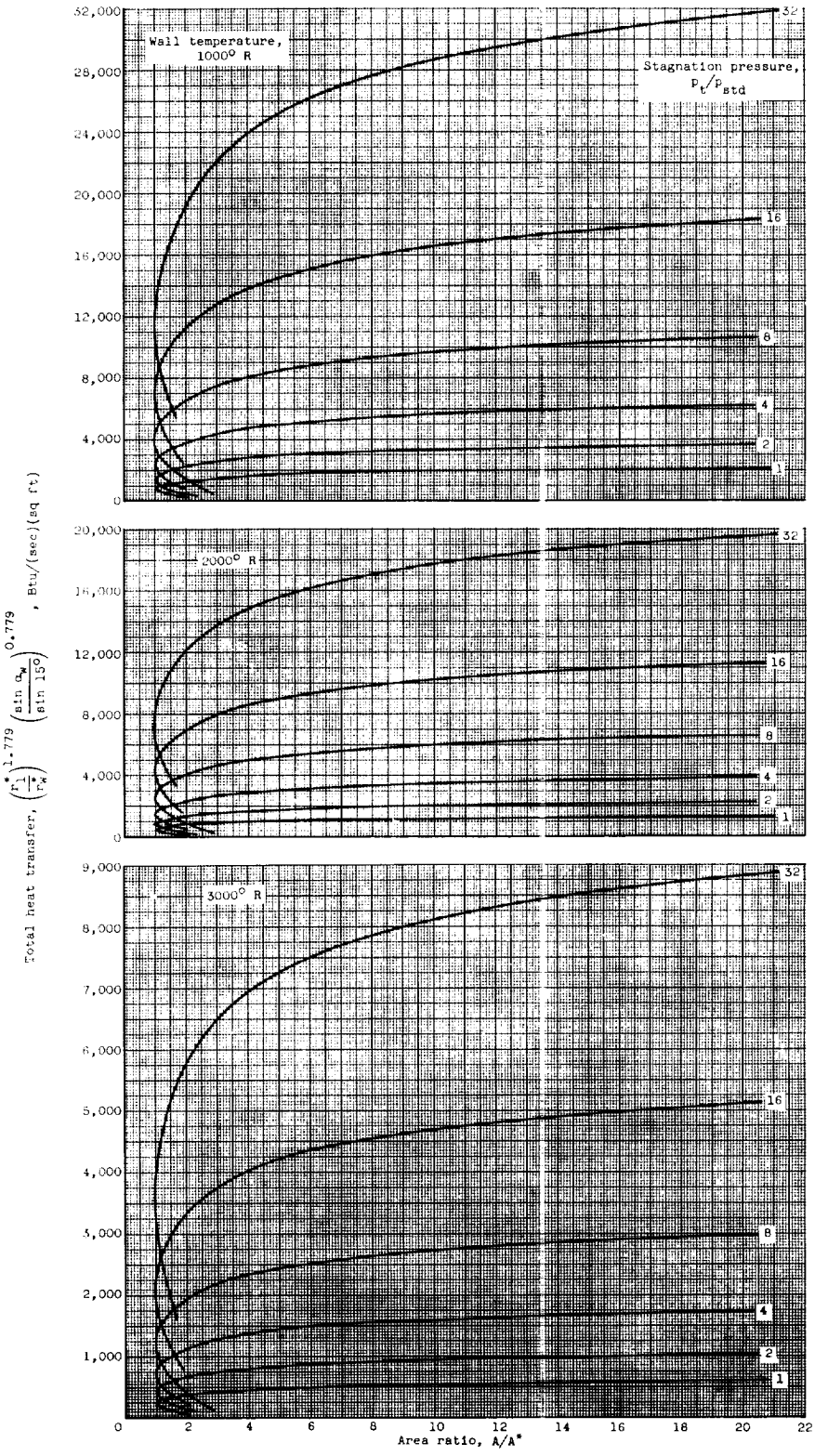

(b) Stagnation temperature, 4000° R.

Figure 9. - Continued. Total heat transfer through nozzle.

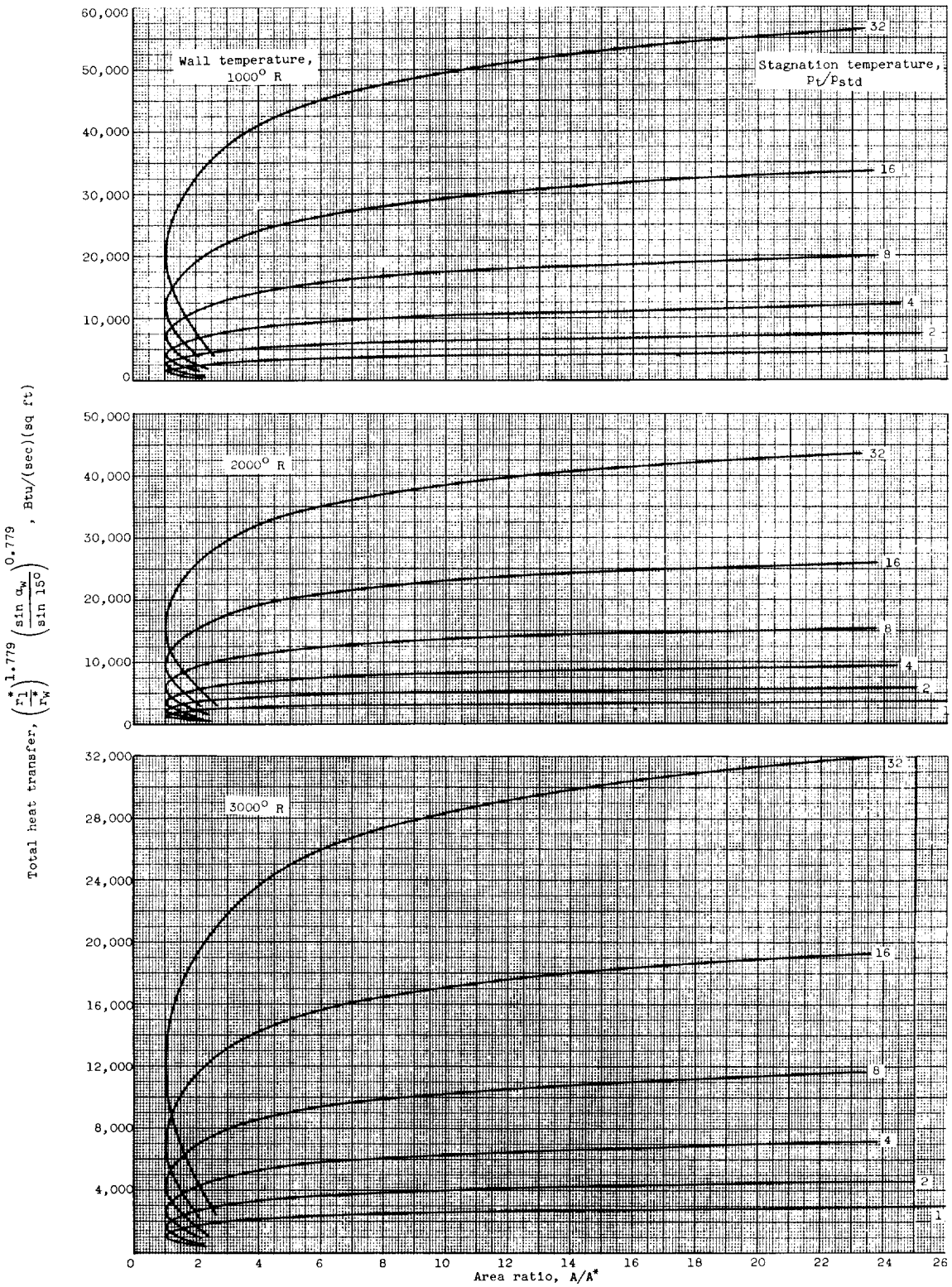

(c) Stagnation temperature, 6000° R.

Figure 9. - Concluded. Total heat transfer through nozzle.

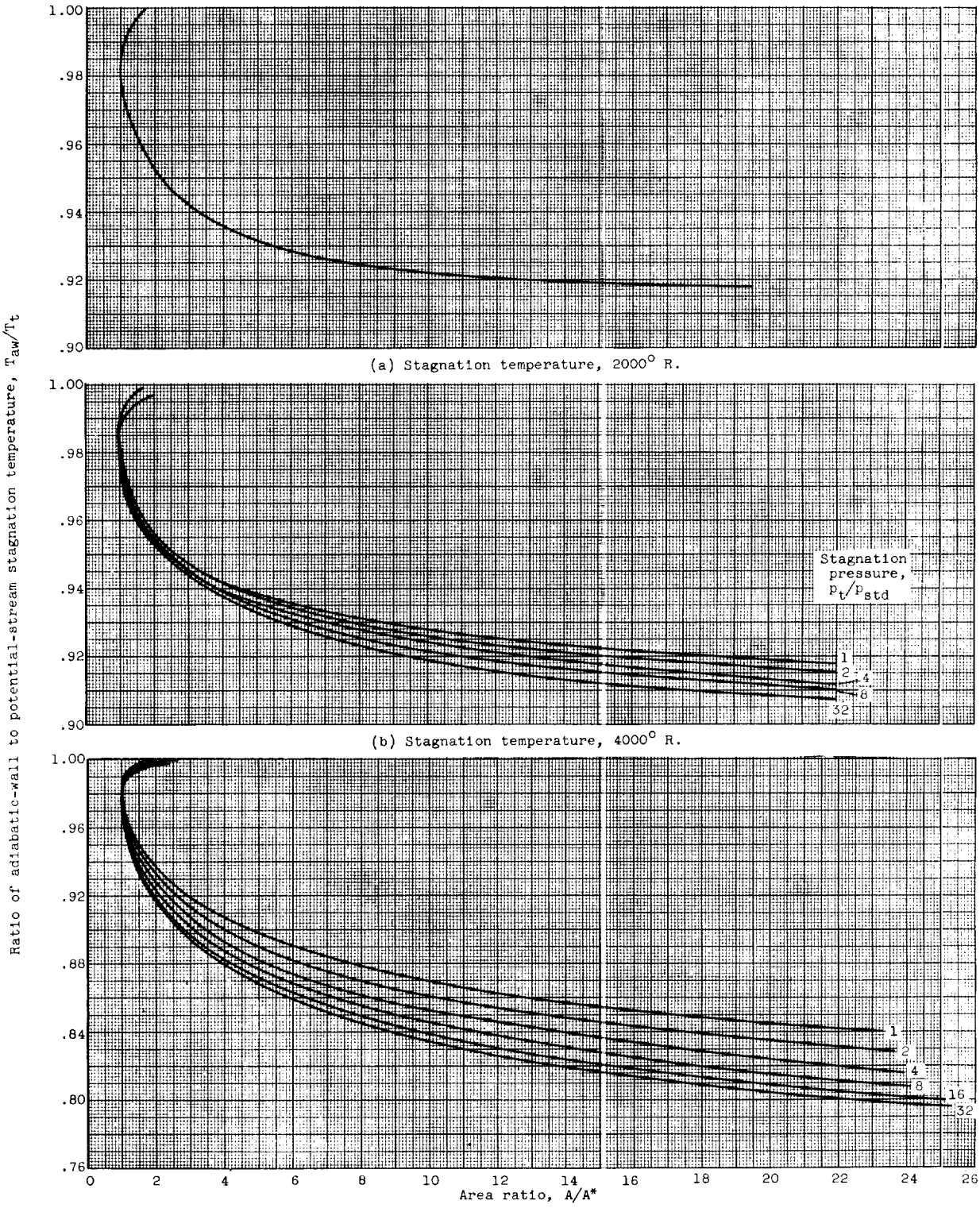

(a) Stagnation temperature, 2000° R.

(b) Stagnation temperature, 4000° R.

(c) Stagnation temperature, 6000° R.

Figure 10. - Adiabatic wall temperature.

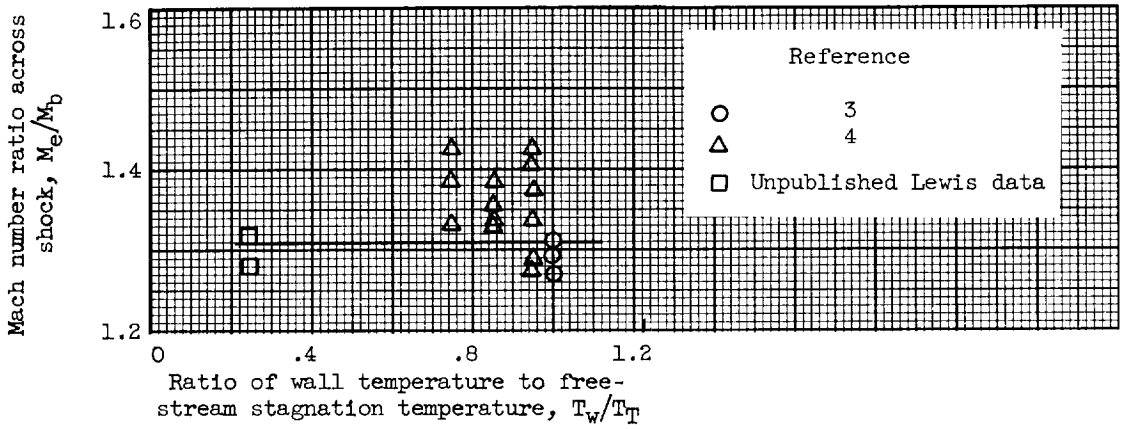

(a) Separation Mach number ratio.

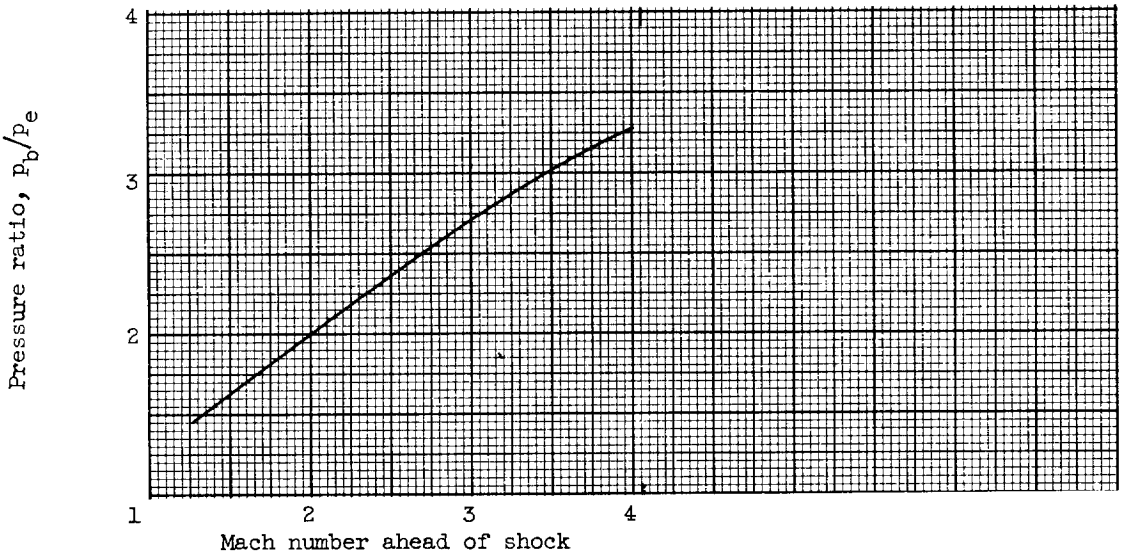

(b) Separation pressure ratio.

Figure 11. - Turbulent boundary-layer separation characteristics.